
Primitive Shape Recognition for Object Grasping

Yunzhi Lin, Chao Tang, Fu-Jen Chu, Ruinian Xu, and Patricio A. Vela¹

Abstract

Shape informs how an object should be grasped, both in terms of where and how. As such, this paper describes a segmentation-based architecture for decomposing objects sensed with a depth camera into multiple primitive shapes, along with a post-processing pipeline for robotic grasping. Segmentation employs a deep network, called *PS-CNN*, trained on synthetic data with 6 classes of primitive shapes and generated using a simulation engine. Each primitive shape is designed with parametrized grasp families, permitting the pipeline to identify multiple grasp candidates per shape region. The grasps are rank ordered, with the first feasible one chosen for execution. For task-free grasping of individual objects, the method achieves a 94.2% success rate placing it amongst the top performing grasp methods when compared to top-down and $SE(3)$ -based approaches. Additional tests involving variable viewpoints and clutter demonstrate robustness to setup. For task-oriented grasping, *PS-CNN* achieves a 93.0% success rate. Overall, the outcomes support the hypothesis that explicitly encoding shape primitives within a grasping pipeline should boost grasping performance, including task-free and task-relevant grasp prediction.

Keywords

Recognition, Grasping, AI Reasoning Methods

1 Introduction

Manipulation is traditionally a multi-step task consisting of sequential actions applied to an object—as determined from perception and planning modules—to be executed by a robotic arm with a gripper. Although it may be taken for granted that object grasping is an easy task based on human grasping capabilities at a young age, high accuracy robot grasping remains a challenging problem due to the diversity of objects that a robotic arm could grasp and the contact dynamics associated to specific robot hand designs. Deep learning has emerged as a strong approach for addressing these issues, however additional research can hopefully better illuminate how to design grasping strategies for robotic manipulators.

In contrast to object-centric approaches, which require creating 3D models or scanning large quantities of real objects (Wohlkinger et al. 2012; Calli et al. 2017) and also require a high accuracy detector, people intuit that objects with similar shapes can be grasped in an object-agnostic manner and that household objects seen in daily life are composed of a limited set of canonical shapes. Based on these two observations, this paper explores the related assertion that *shape is an important property to explicitly encode within a grasping pipeline*. Doing so will promote grasping success.

To validate the assertion, this paper describes the design and evaluation of a more geometric and explicitly shape-centric approach to grasp recognition based on primitive shapes. Primitive shapes offer a powerful means to alleviate data inefficiency and annotation insufficiency (Yamanobe and Nagata 2010; Jain and Argall 2016; Tobin et al. 2017) by abstracting target objects to primitive shapes with *a priori* known grasp options. Previous primitive shape methods represented objects as a single shape from a small library

(Jain and Argall 2016; Eppner and Brock 2013), applied model-based rules to deconstruct objects (Yamanobe and Nagata 2010) or employed Reeb graphs for decomposition (Aleotti and Caselli 2012). As a result, they do not handle novel objects with unmodeled geometry or being the union of primitive shapes. Thus, traditional shape methods neither obtain a high object grasping success rate, nor show the potential to solve more advanced tasks including grasping in clutter and bin picking (Mahler et al. 2019), and task-oriented grasping (Fang et al. 2018). Meanwhile, current state-of-the-art grasping methods using deep networks relegate shape to an implicitly derived internal concept captured through training.

Working from Yamanobe and Nagata (2010)’s model decomposition idea, this paper studies the role of a primitive shapes detector in supporting generalized grasp strategies for household objects. Figure 3 depicts the general concept, with a robot whose objective is to grasp the pot. The pot consists of a handle attached to a container, which maps to stick and cylinder object classes. Grasping the handle can be performed through any grasp from a continuously parametrized set of grasp poses, and likewise for the container component. Awareness of shape informs knowledge of potential grasps for an object. More explicitly stated, *this manuscript explores the effectiveness*

¹Intelligent Vision and Automation Laboratory (IVALab), School of Electrical and Computer Engineering, Institute for Robotics and Intelligent Machines; Georgia Institute of Technology, GA, USA.

Corresponding author:

Yunzhi Lin, Intelligent Vision and Automation Laboratory (IVALab), Georgia Institute of Technology, North Ave NW, Atlanta, GA 30332.
Email: yunzhi.lin@gatech.edu

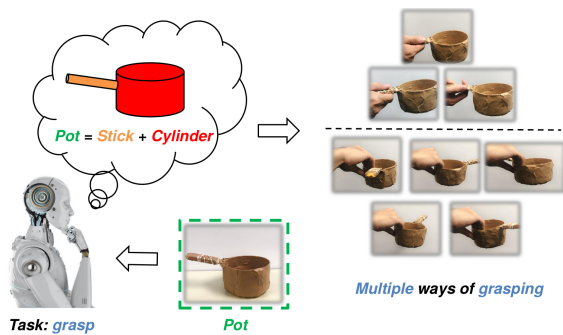


Figure 1. Concept graph of the proposed approach: the robot first infers the primitive shape decomposition of captured household object (e.g. a pot is decomposed into a stick and a cylinder). Grasp family is then applied to each shape, enabling to grasp the object part appropriately under specific contexts.

of primitive shape object decompositions towards the task of grasping objects by leveraging recent results in deep network segmentation to achieve the decomposition. It aims to show that explicit recognition of shape provides an effective means to generate grasp candidates.

1.0.1 Overall Approach. Figure 2 depicts the processing flow for the primitive shape informed grasping pipeline described in this manuscript. Upon receipt of an input depth image, the image contents are segmented into distinct primitive shape categories. Detection and segmentation of these categories exploits the Mask R-CNN (He et al. 2017) instance segmentation deep network trained to segment a depth image according to the primitive shapes it contains. The processing that follows employs traditional grasp methods to generate a grasp candidate from a segmented primitive shape. The post-segmentation process involves shape parameter estimation, pose recovery, grasp family specification, and grasp prioritization or selection via rank scoring. After this final step, the selected grasp is planned and executed. When coupled to a robotic arm, the pipeline identifies primitive shapes within the scene to recover suitable grasp options for objects associated to the primitive shapes.

1.0.2 Training Data. Deep learning for visual processing is data-intensive and requires annotated input/output datasets for training. Consequently, deep learning solutions are fully specified only when the deep network structure and learning processes are specified. Robotics research mitigates the cost of manual annotation for deep learning through the use of programmed simulations (Tremblay et al. 2018a) with automated, known ground-truth annotation capabilities. When combined with domain randomization (Tobin et al. 2017, 2018), the resulting training datasets permit translation of the learnt relationships to input data capture from actual sensors. In some cases, there is still a performance gap arising from the distribution mismatch between the training data set and the deployment input data. Reducing the mismatch is known as domain alignment (Sankaranarayanan et al. 2018). Here, data distribution gaps are tackled through both randomization and alignment.

Alignment is addressed in a bi-directional manner by corrupting the simulated data and denoising the depth image data. The intent is to introduce real sensor artifacts that cannot be removed in the simulated images, and

to denoise the real images to match the simulated images. Randomization is addressed through the use of synthetic ground truth data based on parametrized sets of primitive shape classes and their parametrically defined grasp families. The parametric models permit automatic synthesis of diverse input scenes with their matching output grasps, thereby avoiding extensive manual annotation. The shape classes are sufficiently representative of object parts associated to household objects yet low enough in cardinality that grasp family modeling is quick. Simulated domain randomization and data corruption generates a large synthetic dataset composed of different primitive shapes combinations, quantities, and layouts. The automated ground truth generation strategy rapidly generates input/output data.

1.0.3 Contribution. This study extends a previous conference version (Lin et al. 2020) beyond proof-of-concept and focuses on the value of explicitly encoding shape information. It improves the dataset generation strategy and replaces the post-processing components downstream of shape segmentation with improved model-based approaches based on best practice. Experimental confirmation includes more categories of objects and additional grasping tests that demonstrate the robustness and value of primitive shapes.

The main contribution is the testing and confirmation of the hypothesis that explicitly encoding shape primitives within a grasping pipeline boosts grasping performance. In particular, executing the deep-learning enabled pipeline of Figure 2, which is detailed in Sections 6-7, on an actual 7-DOF robotic manipulator (Section 6) confirms that shape primitives provide an effective means to generate grasp candidates. The grasping pipeline achieves one of the highest success rates on individual objects amongst parallel plate gripper, or equivalent, manipulation systems using a single-shot grasp recognition strategy. Published works with higher success rates employ an eye-in-hand visual servoing strategy (using multiple images), a suction cup, or a dual-gripper strategy with a suction cup and a parallel plate gripper, with the suction cup being the dominant factor leading to the high success rates (Mahler et al. 2019). As such, the first of them exploits the temporal regularity possible through repeated measurements and predictions, while the latter two address the grasping and grasp closure problem through an alternative grasping mechanism. Additional studies demonstrate primitive shapes have some robustness under different operational settings (i.e., camera viewpoint and light clutter). More importantly, primitive shapes enable the recognition of specific shape regions, which paves the way for task-oriented grasping or purposeful manipulation. The studies provide evidence in favor of an explicit shape primitive recognition module for grasp recognition strategies. They also suggest areas for improvement in the primitive shape grasping pipeline.

2 Related Work

Grasping is a mechanical process involving intentional contact between a robot end-effector and an object. It can be mathematically described from prior knowledge of the target object’s properties (geometry, hardness, etc.), the hand contact model, and the hand dynamics (Murray 2017; Bicchi and Kumar 2000). Mechanics-based approaches with

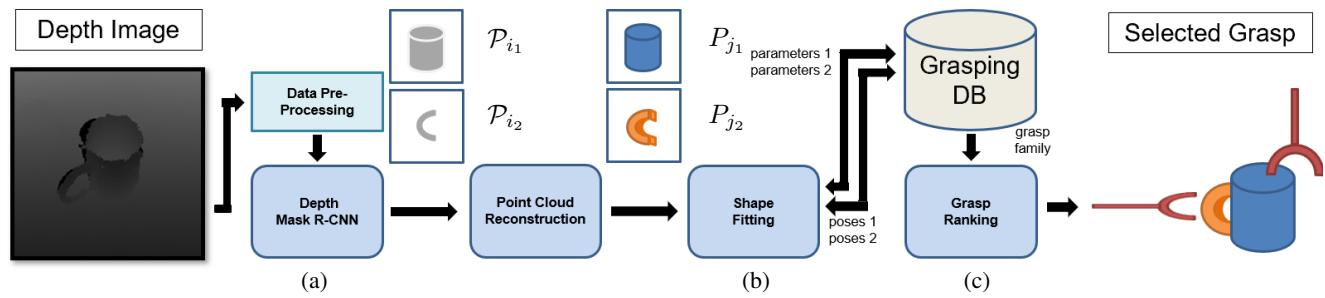


Figure 2. The proposed deep network, segmentation-based pipeline. (a) From monocular depth input, objects are segmented into primitive shape classes, with the object to grasp extracted and converted into primitive shape point clouds. (b) Shape pose and parameter estimation, grasp scoring, and grasp selection processes follow. The best matching shape pose and parameter per primitive shape are identified. (c) Candidate grasps are priority ranked and tested for feasibility with the first feasible grasp chosen for physical robot executions.

analytical solutions work well for some objects but cannot successfully apply to other, often novel, target objects (Tung and Kak 1996; Prattichizzo et al. 2012; Rosales et al. 2012). Grasp scoring methods augmented by point cloud processing overcome some of these limitations (Aleotti and Caselli 2012; ten Pas et al. 2017). However, analytical models cannot cover the parametric variation associated to all potential objects to grasp. In hopes of permitting more robust generalization over model-based methods, efforts have gone into data-driven approaches using machine learning (Bohg et al. 2014) as well as combined approaches employing analytic scoring with *image-to-grasp* learning (Mahler et al. 2017). Contemporary state-of-the-art grasping solutions employ deep learning (Caldera et al. 2018) and leverage available training data.

2.1 Deep Learning Strategies

Deep learning strategies primarily take one of three types. The first type exploits the strong detection or classification capabilities of deep networks to recognize candidate structured grasping representations (Watson et al. 2017; Park and Chun 2018; Chu et al. 2018; Satish et al. 2019). The most common representation is the $SE(2) \times \mathbb{R}^2$ grasp representation associated to a parallel plate gripper. As an oriented rectangle (Asif et al. 2019) or a pair of keypoints (Wang et al. 2021; Xu et al. 2021), there is an underlying assumption of a top-down view such that the grasp representation directly maps to a top-down grasp to execute. As a perception problem, recognition accuracy is high (around 95% or higher), with a nearly comparable performance during robotic implementation (around 90% and up). Training involves image/grasp datasets obtained from manual annotation (Lenz et al. 2015) or simulated grasping (Depierre et al. 2018; Satish et al. 2019). Related to this category is, DexNet (Mahler et al. 2017), which uses random sampling and analytical scoring followed by deep network regression to output refined, learnt grasp quality scores for grasp selection. By using simulation with an imitation learning methodology, tens of thousands to millions of annotations support DexNet regression training. Success rates vary from 80% to 93% depending on the task. Another trend is to work in the full $SE(3) \times \mathbb{R}^3$ space. It removes the constraint of 2D grasping that requires grasping aligned with the tabletop frame or the image plan and optical axis. As a result, 3D grasp supports greater grasp diversity

and more advanced manipulation tasks. Recent approaches process the 3D point cloud input either in a discriminative or a generative manner. Discriminative methods (ten Pas et al. 2017; Liang et al. 2019) sample grasp candidates and then rank them according to grasp quality network or other heuristic evaluations. On the other hand, generative approaches (Mousavian et al. 2019; Qin et al. 2020; Ni et al. 2020; Wu et al. 2020) directly regress 6-DoF grasp configurations. They claim to be a robust choice in cluttered scenes.

The second type replaces annotation or simulation with actual experiential data coupled to deep network reinforcement learning methods (Levine et al. 2018; Zeng et al. 2018), when sufficient resources are available. It is a preferred option when the ground truth annotations are hard to obtain. Grasping solutions based on simulation or experience tend to be configuration-dependent; they usually learn for specific robot and camera setups.

The third type is based on object detection or recognition (Bohg et al. 2014). Again, recent work employs deep learning to detect objects and relative poses to inform grasp planning (Tremblay et al. 2018b; Xiang et al. 2018; Peng et al. 2019; Wang et al. 2019). Others may perform object-agnostic scene segmentation to differentiate objects followed by a DexNet grasp selection process (Danielczuk et al. 2019) or a GraspNet grasp generation process (Mousavian et al. 2019). Like Danielczuk et al. (2019), this paper focuses on where to find candidate grasps as opposed to grasp quality scoring.

Although deep learning grasp methods have achieved great success shown in the aforementioned discussion, they still suffer from two related problems: sparse grasp annotations or insufficiently rich data (i.e., covariate shift). The former can be seen in Figure 3, which shows an image from the Cornell dataset (Jiang et al. 2011) and another from the Jacquard dataset (Depierre et al. 2018). Both lack annotations in graspable regions due to missing manual annotation or a false negative in the simulated scenario (either due to poor sampling or incorrect physics). Sampling insufficiency can be seen in Satish et al. (2019), where the DexNet training policy was augmented with an improved (on-policy) oracle to provide a richer sampling space. Yet, sampling from a continuous space is bound to under-represent the space of possible options, especially for higher parametric grasp space dimensions.

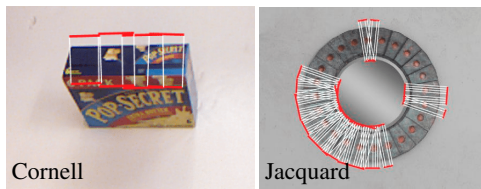


Figure 3. Grasp annotation data with missing grasp candidates.

2.2 Primitive Shapes

This paper proposes to more fully consider shape primitives (Miller et al. 2003) due to their known, parametrized grasp families (Yamanobe and Nagata 2010; Shiraki et al. 2014). The parameterized families provide a continuum of grasp options rather than a sparse sampling. A complex object can be decomposed into parts representing distinct surface categories based on established primitives.

The primitive shapes idea has a long history dating back to the 1970s, when Marr and Nishihara (1978) illustrated the concept of decomposing a human 3D model into combinations of cylinders. Since then, researchers in the computer vision community have advanced on the idea (Kaiser et al. 2019), with approaches based on RANSAC-enabled extensions with randomized fits with maximal consensus (Schnabel et al. 2007), primitive-driven region growing algorithms that extract connected components with neighborhood information (Attene and Patanè 2010), and clustering approaches for detecting simple geometric primitives (Holz et al. 2011). More recent progress further demonstrating the potential of primitive shapes introduces different deep neural network designs such as a vowel-based network to generate primitives (Tulsiani et al. 2017), an image-based network combined with Conditional Random Field (CRF) (Kalogerakis et al. 2017), and point-based network with differentiable primitive model estimator (Li et al. 2019). However, those methods generally took a 3D model or a point cloud randomly sampled on a model’s surface as the input (Paschalidou et al. 2019, 2020), even required fine-grained labels to train the networks (Sharma et al. 2020), which is not as feasible to achieve for grasping.

Past research in the robotic grasping field explored shape primitive approaches in the context of point cloud processing (Aleotti and Caselli 2012) and fitting for the cases of superquadric (Goldfeder et al. 2007; Vezzani et al. 2017; Xia et al. 2018; Hachiuma and Saito 2020) and box surfaces (Huebner and Kragic 2008). In most cases, the entire sensor-scanned object point cloud is required for shape segmentation and grasp selection. Existing approaches also model objects as individual primitive shapes (Eppner and Brock 2013; Jain and Argall 2016; Vezzani et al. 2017; Fang et al. 2018), which do not exploit the potential of primitive shapes to generalize to unseen/novel objects. Deep network approaches for shape primitive segmentation to inform grasping do not appear to be well studied.

2.3 Domain Randomization

Deep learning is data-intensive, which translates to unwieldy manual annotation efforts. As noted earlier, robotics research employs simulation and synthetic data generation whenever possible (Levine et al. 2018; Zeng et al. 2018), e.g., DexNet

uses simulation to generate grasp quality test data (Mahler et al. 2017; Satish et al. 2019). Thus, the data generation component is considered part of the solution. Improvements in simulation and rendering fidelity (Denninger et al. 2019; Morrical et al. 2021) permit the generation of large scale photo-realistic datasets with demonstrated performance improvements (Hodaň et al. 2019). However, simulation introduces a domain gap, or distribution shift, because the training signals and the true input signals differ. The gap can be overcome through domain randomization and consideration of how the two signals differ (Prakash et al. 2019).

Domain randomization is a prevalent method in the robotics simulation field. It strives to permit networks trained from simulated data to apply to real-world domains without additional real image input (Tobin et al. 2017; Peng et al. 2018; Andrychowicz et al. 2020). Since domains can be parametrically complex, structured domain randomization helps to regulate multiple parameters in a more organized manner through a probability distribution map (Prakash et al. 2019). In some cases, it might be possible to establish which parameters are more useful to bridge the domain gap through a guided domain randomization approach (Zakharov et al. 2019).

Typically, domain randomization solutions are designed for RGB inputs. This paper makes use of depth images as inputs, which requires modifying the existing methods or identifying depth-specific approaches. Relative to color imagery, depth imagery has a less severe gap more readily addressed. One source of the mismatch for modern robotics simulation engines (Rohmer et al. 2013; Community 2018) is that they render and simulate virtual environments quite cleanly, often leading to sensor imagery with less defects than real sensors. Depth sensors like the Kinect v1 loses details and introduces noise during the depth capture (Planche et al. 2017; Sweeney et al. 2019), while also having shadow effects from the active illumination, leading to a persistent distribution shift between the simulated depth data and sensed depth data. Mechanisms to correct for this shift are needed for deep learning to be used for primitive shape segmentation. Here, addressing domain shift focuses on the variation of the placed objects as a randomization strategy and employs bi-directional alignment to reduce sensing-based gaps. By incorporating a specially-designed primitive shapes family and targeting household objects, the ground truth generation strategy reduces the domain shift.

3 Grasping from Primitive Shapes Recognition

The intent behind this investigation is to explore the potential value of using deep networks to segment a scene according to the surface primitives contained within it, thereby establishing *where* to grasp. Once the object or region to grasp is known, post-processing recovers the shape geometry and the grasp family associated to the shape, to establish *how* to grasp. The state-of-the-art instance segmentation deep network Mask R-CNN (He et al. 2017) serves as the backbone network for converting depth images into primitive shape segmentation images. Importantly, a synthetically generated training set using only shape primitives in concert

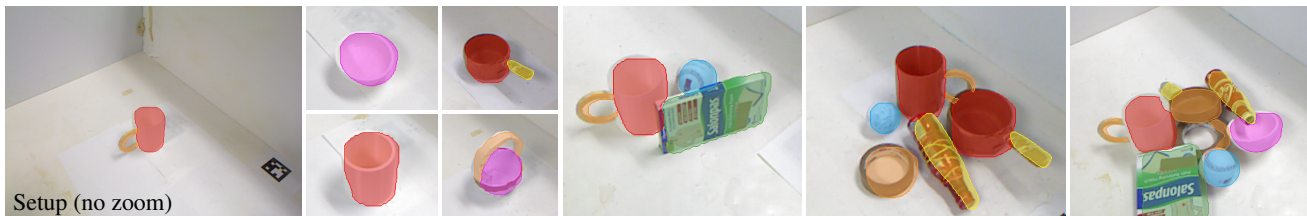


Figure 4. Sample segmentation outcomes for test scenarios consisting of individual and multiple objects (zoomed and cropped images).

with domain randomization (Tobin et al. 2017) covers a large set of scene visualizations. The ability to decompose unseen/novel objects into distinct shape regions, often with explicitly distinct manipulation affordances, permits task-oriented grasping (Fang et al. 2018).

The vision-based robotic grasping problem here presumes the existence of a depth image $\mathcal{D} \in \mathbb{R}^{H \times W}$ (H and W are image height and width) capturing a scene containing an object to grab. The objective is to abstract the scene into a set of primitive shapes and generate grasp configurations from them. A complete solution involves establishing a routine or process, f , mapping the depth image \mathcal{D} to a grasp $\mathcal{G} = f(\mathcal{D}) \in SE(3)$. The grasp configuration $\mathcal{G} \in SE(3)$ specifies the final pose in the world frame of the end-effector.

Per Figure 2, the process is divided into three stages. In the first stage, the depth image \mathcal{D} gets segmented according to defined primitive shape categories indexed by the set I . The primitive shape segmentation images are \mathcal{P}_i for $i \in I$. The segmentation \mathcal{P}_i and the depth image \mathcal{D} generate segmented point clouds in 3D space for the primitive surfaces attached to the label i . In the second stage, when the grasp target is established, the surface primitives attached to the target grasp region are converted into a corresponding set of primitive shapes P_j in 3D space, where j indexes the different surface primitive segments. In the third stage, the parametrized grasp families of the surface primitives are used to generate grasp configurations \mathcal{G}_α for $\alpha \in \mathbb{N}^+$. A prioritization process leads to rank-ordered grasps with the first feasible grasp being the one to execute. This section details the three stages and the deep network training method.

4 Primitive Shape Segmentation

The proposed approach hypothesizes that commonly seen household objects can be decomposed into one or more primitive shapes. After studying several household object datasets (Calli et al. 2017; Chen et al. 2003; Funkhouser et al. 2003; Shilane et al. 2004), the chosen primitive shapes were: *Cylinder*, *Ring*, *Stick*, *Sphere*, *Semi-sphere*, and *Cuboid*. A deep learning procedure will be described for creating a network based on Mask-RCNN (He et al. 2017) with primitive shape segmentation outputs from depth image inputs. Doing so requires providing both the annotated training set, and the training technique. Sections 4.1 and 4.2 detail method used to synthetically generate depth images and known segmentations from the parametric shape classes. Section 4.3 describes the training procedure for generating the Mask-RCNN network that will decompose an input depth image into a set of segmentations reflecting hypothesized primitive shapes. To gain a sense for the output structure of the trained primitive shape segmentation network (PS-CNN),

Table 1. Primitive Shape Classes

Class	Parameters	Range (unit: cm)
Cylinder	(r_{in}, r_{out}^*, h)	$r_{in} \in [3, 7], \sigma_1 = 0.3$ $h \in [5, 10], \sigma_2 = 0.5$
Ring	(r_{in}, r_{out}^*, h)	$r_{in} \in [1.4, 4], \sigma_1 = 0.2$ $h \in [0.8, 2.4], \sigma_2 = 0.1$
Stick	(r_{in}, r_{out}^*, h)	$r_{in} \in [0.8, 1.5], \sigma_1 = 0.1$ $h \in [4, 10], \sigma_2 = 0.5$
Sphere	r	$r \in [2, 5], \sigma = 0.2$
Semi-sphere	r	$r \in [2, 5], \sigma = 0.2$
Cuboid	(h, w, d)	$h, w, d \in [2, 12], \sigma = 0.5$

r - radius, r_{in} - inner radius, r_{out} - outer radius
 h - height, w - width, d - depth

*To simplify generation, r_{out} is set to be 1.15 times r_{in} .

Figure 4 depicts several segmentations for different input depth images overlaid on the corresponding, cropped RGB images. The color coding is red: *Cylinder*, orange: *Ring*, yellow: *Stick*, blue: *Sphere*, purple: *Semi-sphere*, and green: *Cuboid*. For individual, sparsely distributed, and clustered objects, PS-CNN captures the primitive shape regions and classes of the sensed objects.

4.1 Dataset Generation

The value of using primitive shapes is in the ability to automatically synthesize a vast library of shapes through gridded sampling within the parametric domain of each class. This section describes what parameters are varied to synthetically generate input imagery with known segmentation outcomes, from the V-REP simulation software (Rohmer et al. 2013), see Figure 5. Based on the hypothesis that a dataset with diverse combinations of primitive shapes could induce learning generalizable to household objects, the dataset generation procedure consists of the following degrees of freedom: (1) camera pose setup: a principle camera fixed to a specific pose or canonical view while four other assistant cameras are instantiated with random relative poses around the principle camera; (2) primitive shape parameters; (3) placement order; (4) placement flag, for which there are two options: one to place all the objects close together, one to scatter them; (5) initial placement location assigned in a Gaussian distribution; (6) mode of placement, for which there are three modes: *free-fall*, *straight up from the table-top*, and *floating in the air*; and (7) initial orientation.

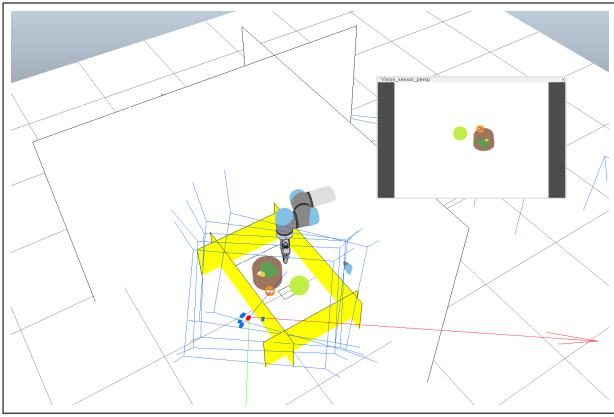


Figure 5. Experimental setup in the simulator, where the red represents the principle camera and the blue represents the assistant cameras.

Regarding the camera pose parameters, the principle camera view provides an input image from the expected perspective associated to the nominal configuration. The addition of four assistant cameras generates varied viewpoints should the configuration be off. It also provides some variation equivalent to translating the object placement by a small amount. For each primitive shape, a specific parametric model determines its geometry. Table 1 lists the parameter coordinates (middle column) for each primitive shape class. The *Cylinder*, *Ring*, and *Stick* are modeled to have r_{in} , r_{out} and h parameters, where r_{out} is fixed to be 1.15 times r_{in} for simplicity. Those classes could be considered as three subsets of cylinder-like shapes with different radius-to-height ratios. The *Sphere* and *Semi-sphere* are only defined by a radius value. The *Cuboid* is modeled by its three main edges. All of the parameters are limited to a particular range, grid discretized according to σ . Every scene generated has one randomly generated instance of each primitive class, with the insertion order randomly determined.

Once the core parameters for the camera and the primitive shapes have been established, the next step is to place the shapes within the scene. The placement flag is randomly chosen between the two options following a ratio of 4:1, indicating a preference for objects to be placed close together to generate more complex combinations. The scatter option often isolates the objects to create loose clutter. To place objects close to each other, the first option assigns all the objects the same mean placement location, while the second option would individually assign the objects a mean placement location within the scene. The actual placement of the objects will be based on The initial placement location is generated according to a Gaussian distribution where the mean is set to be the placement location center and the variance is set to be 0.15m. The placement mode is randomly determined for each shape inserted. The initial orientation is uniformly randomly determined within a bounding volume above the table-top.

Through random selection, 300k scenes of different primitive shapes combinations are generated. A typical scene is shown in Figure 5. For each instance, RGB and depth image pairs are collected. Shape color coding provides segmentation ground truth and primitive shape ID. The process samples a sufficiently rich set of visualized shapes

once self-occlusion and object-object occlusion effects are factored in.

4.2 Domain Alignment between Simulation and Reality

State-of-the-art simulators (Rohmer et al. 2013; Community 2018) benefit data generation by automating data collection in virtual environments, but do so using idealized physics or sensing. Some physical effects are too burdensome to model. To alleviate this problem, the images from both sources, the simulation and the depth sensor, are modified to better match. The objective is to minimize the corrections applied, therefore the first step was to reduce or eliminate the sources of discrepancies. Discrepancy reduction involves configuring both environments to match, which includes the camera’s intrinsic and extrinsic parameters, and the background scene. Comparing images from both sources, the main gap remaining is the sensing noise introduced by the low-fidelity Kinect v1 depth sensor (Planche et al. 2017; Sweeney et al. 2019). The Kinect has occlusion artifacts arising from the baseline between the active illuminator and the imaging sensor, plus from measurement noise. The denoising process includes temporal averaging, boundary cropping, and median filtering, in that order. Once the Kinect depth imagery is denoised, the next step is to corrupt the simulated depth imagery to better match the visual characteristics of the Kinect. The primary source of uncertainty is at the depth edges or object boundaries due to the properties of the illuminator/sensor combination. The simulated imagery should be corrupted at these same locations. The simulated environment has both a color image and a depth image. The color image is designed to provide both the shape primitive label and the object ID, thereby permitting the extraction of object-wise boundaries. After establishing the object boundary pixels, they are dilated to obtain an enlarged object boundaries region, then an oil painting filter (Sparavigna and Marazzato 2010; Mukherjee et al. 2014) corrupts the depth data in this region. Considering that manipulation is only possible within a certain region about the robotic arm, the depth values from both sources were clipped and scaled to map to a common interval. Figure 6 depicts this bi-directional process showing how it improves alignment between the two sources.

4.3 Data Preprocessing and Training

Per §4.2, the simulated depth images are re-scaled then corrupted by a region-specific oil-painting filter. To align with the input of Mask R-CNN, the single depth channel is duplicated across the three input channels. The ResNet-50-FPN as the backbone is trained from scratch on corrupted depth images in PyTorch 1.1. It runs for 250,000 iterations with 4 images per mini-batch. The primitive shape dataset is divided into a 83%/17% training and testing splits. The learning rate is set to 0.02 and divided by 10 at iterations 50000, 100000, and 180000. The workstation consists of a single NVIDIA 1080Ti (Pascal architecture) with cudnn-7.5 and cuda-9.0. Dataset generation takes 95 hours, and training takes 55 hours (150 hours in total).

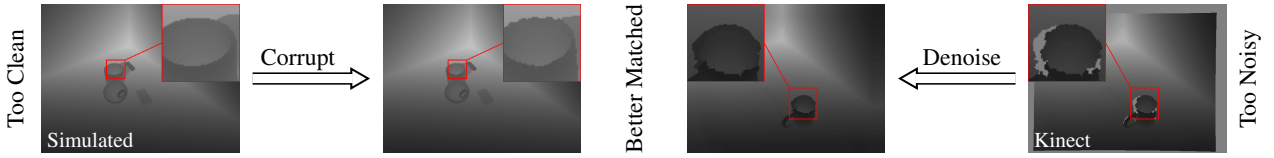


Figure 6. Bi-directional image filtering to align training data and real data. An oil painting filter applied to training imagery simulates the noise of the Kinect depth sensor. Temporal averaging and spatial median filtering regularize the Kinect depth image during run-time.

Table 2. Performance of PS-CNN on 3D printed primitive shapes

	Original	Corrupted
Cylinder	0.822	0.834
Ring	0.907	0.902
Stick	0.795	0.824
Sphere	0.591	0.842
Semi-sphere	0.905	0.919
Cuboid	0.916	0.915
All	0.823	0.872

4.4 Vision Evaluation Metrics

Evaluation of the proposed pipeline consists of testing on novel input data as purely a visual recognition problem, followed by testing on the experimental system. For the visual segmentation evaluation, the segmentation accuracy is computed by F_{β}^{ω} (Margolin et al. 2014):

$$F_{\beta}^{\omega} = (1 + \beta^2) Pr^{\omega} \cdot Rc^{\omega} / (\beta^2 \cdot Pr^{\omega} + Rc^{\omega}). \quad (1)$$

where Pr^{ω} is weighted precision and Rc^{ω} is weighted recall. β signifies the effectiveness of detection, which is set to 1 by default.

4.5 Vision Result

Segmentation tests are performed on a set of 3D printed primitive shapes and compared to manual segmentations. The tested implementations include a network trained with the original simulated images (no corruption) and with the oil-painting corrupted images. Per Table 2, the F_{β}^{ω} segmentation accuracy improved from 0.823 to 0.872 (ranges over $[0, 1]$), with the primary improvement sources being for the *sphere* shape class followed by the *stick class*. The segmentation accuracy is sufficient to capture and label significant portions of an object’s graspable shape regions, see Figure 4.

5 From Primitive Shapes to Grasp Candidate

5.1 Shape Fitting

Given a target object region to grasp, the intersecting shape primitive regions are collected and converted into separate partial point clouds. For each region and its hypothesized shape class, Principal Component Analysis (PCA) is first adopted to predict a coarse primary vector for reference. Random Sample Consensus (RANSAC) then estimates the pose and parameter of the partial point cloud over the shape model parameter space of the primitive shape. The

outputs inform an object shape model for hypothesizing the candidate grasp family for each object. This matching step is depicted in Figure 2(b). Although the estimated geometric primitives may not perfectly match the target region, the downstream pipeline is robust to errors that do not significantly impact the grasp’s gripper properties (e.g., opening width). For more details on this standard shape fitting process, see the Supplemental Material at Lin et al. (2021). Figure 7 depicts the process of taking the depth image (a) and generating a primitive shape segmentation (b), from which each shape region is segmented out from the point cloud (c) to give a set of point clouds (e)-(h) that correspond to an object or an object part to grasp. In the figure, all of the object maps to a single primitive shape. Figure 9 and Section 7.4 includes cases where objects consist of two primitive shape classes.

5.2 Grasp Family

The premise behind this work is that knowledge of shape informs grasping opportunities. Simple shapes have known grasp options. This section describes how estimating and registering recognized primitive shape models in the scene permits recovery of one or more grasp families corresponding to each recognized shape. Each primitive shape class has a unique design for its grasp families. The configurations are based on the geometry of the primitive shape and of parallel grippers, which are parametrically generated based on shape symmetries. This idea can be extended to other types of grippers. Example shape-based grasp configurations are depicted in Figure 8 for reference.

The grasp family design is as follows:

- 1) *Cylinder*: There are two members corresponding to grasping from the top or from the bottom, with the free parameter being rotation about the cylinder axis. Another member corresponds to grasping from the side (the jaw plane is perpendicular to the principal axis of the cylinder), with the free parameters being the translation along and rotation about the principle axis;
- 2) *Ring*: Similar to the cylinder, a ring can be grasped from the top/bottom/side as well. However, the jaw plane is parallel to circular plane of the ring when approaching from the side;
- 3) *Stick*: A restricted case of the cylinder that can only be grasped from the side;
- 4) *Sphere*: We have two members for the sphere, which correspond to grasping from the top or the side. The free parameter is the rotation about the principal axis of the shape;
- 5) *Semi-sphere*: Unlike the sphere, the semi-sphere can only be grasped from the top while the remaining parameters remain the same;
- 6) *Cuboid*: For the cuboid, the gripper can approach all six facets vertically or horizontally, generating

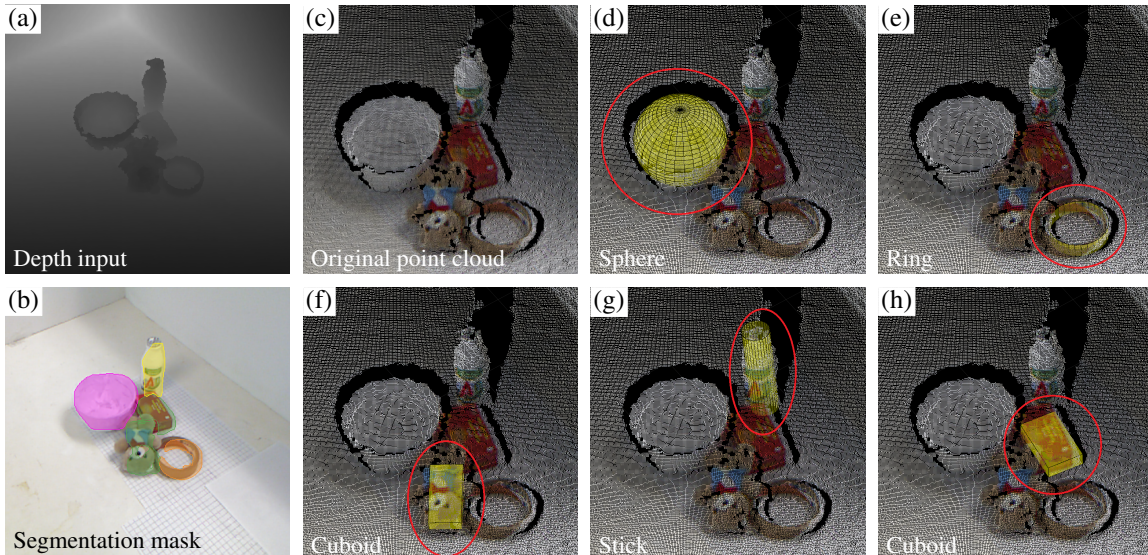


Figure 7. Shape fitting for a multi-object scene (zoomed and cropped images). The target shape fitting result is underlined by red circle.

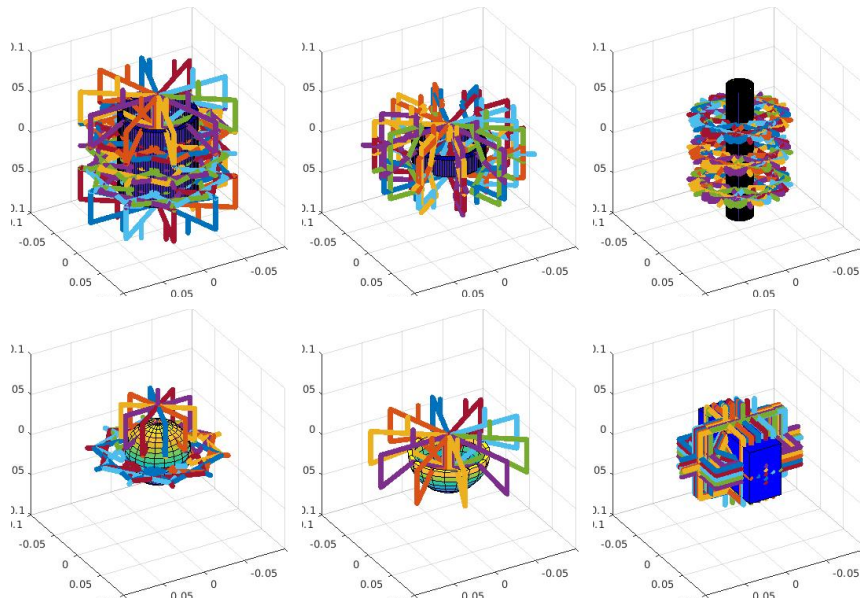


Figure 8. Grasp family for Cylinder, Ring, Stick, Sphere, Semi-sphere, and Cuboid (from left to right, top to bottom).

twelve members (6×2) in total. The free parameter is translation along a single axis in the face plane.

Under ideal conditions (e.g., floating object, no occlusion, no collision, and reachable), all the grasp configurations described above would be possible. However, only a subset of grasps can be feasible in reality when taking more factors into account. Importantly, when trying to grasp object lying on a tabletop surface, the gripper may collide with the tabletop plane if the grasp configuration is too close to the target object. To deal with this challenge, we introduce a specific post-processing step for small objects, where the corresponding grasp family is generated away from the target shape along the computed grasp’s body z-axis. Additionally, three options (small/medium/large) are employed to approximate the best opening width for each grasp candidate. The association is based on the primitive shape class and the grasp family class, while the width

parameters are set empirically according to the gripper geometry.

Adopting the idea of grasp families for primitive shapes avoids issues associated to incomplete annotations or sparse sampling of the grasp space. Since the geometry of each shape is known, the predicted grasp family is robust under different settings (modulo the weight distribution of the object).

5.3 Grasp Prioritization and Selection

The final step prior to execution is to select one grasp from the set of candidate grasps. DexNet 2.0 (Mahler et al. 2017) was explored as a means to score the grasps, but performance degraded as our camera setup was not of a top-down view. Instead, a simple geometric grasp prioritization scoring function was used inspired by GPD grasp ranking (ten Pas et al. 2017). It considers the required pose of the hand

$\mathcal{G} = \mathcal{G}_h^W$ relative to the world frame (which is located at the manipulator base), the dimensions of hand versus the targeted shape, point cloud occupancy, and collision. The prioritization scheme prefers dimension-compatible and collision-free grasps to minimize translation, maximize the volume of point cloud within the gripper closing region, and favor approaching from above due to the manipulator elbow-up geometry. The highest-ranked grasp with a feasible grasping plan is the grasp selected.

The composite grasp prioritization score consists of contributions from rotation, translation, occupancy, dimension-compatibility, and collision of a candidate grasp pose. The translation score contribution depends on the length of the translation element (i.e., the distance from the world/base frame). Define the translation cost as $C_{trans}(T) = \|T\|$, where T is the translation interpreted to be a vector in \mathbb{R}^3 . The rotational contribution regards the equivalent quaternion $\mathbf{q} \in SO(3)$ as a vector in \mathbb{R}^4 and applies the following positive, scalar binary operation to obtain the orientation grasp cost:

$$C_{rot}(\mathbf{q}) = \vec{w} \odot \vec{q}, \quad \text{where } \vec{w} = (0, \omega_1, \omega_2, \omega_3)^T, \omega_i > 0, \quad (2)$$

with $\vec{a} \odot \vec{b} \equiv |a^1 b^1| + |a^2 b^2| + |a^3 b^3| + |a^4 b^4|$. This cost prioritizes vertical grasps by penalizing grasps that do not point down. Alternative weightings are possible depending on the given task, or the robot configuration.

The rotation and translation costs are computed for all grasp candidates, then converted into scores by normalizing them over the range of obtained costs,

$$\begin{aligned} s_{rot}(C_{rot}) &= 1 - \frac{C_{rot} - C_{rot}^{min}}{C_{rot}^{max} - C_{rot}^{min}} \\ s_{trans}(C_{trans}) &= 1 - \frac{C_{trans} - C_{trans}^{min}}{C_{trans}^{max} - C_{trans}^{min}} \end{aligned} \quad (3)$$

where $.^{min}$ and $.^{max}$ superscripts denote the min and max over all grasps, respectively.

We also take grasp stability into consideration. Let $B(\mathcal{G})$ denotes the volume occupied by \mathcal{G} when the gripper is fully open and let $C(\mathcal{G})$ denotes the volumetric region swept out by the gripper when closing. The occupancy score s_{occ} , which represents the volume of point cloud within the $C(\mathcal{G})$, is calculated by

$$s_{occ} = C(\mathcal{G}) \cap P_j. \quad (4)$$

Both of the dimension score s_{dim} and the collision score s_{col} are binary-valued. s_{dim} is set as zero if the estimated shape dimension exceeds the gripper's maximal opening range while s_{col} is set as zero if $B(\mathcal{G}) \cap P_j \neq \emptyset$. The final composite score is:

$$\begin{aligned} \gamma_g(s_{rot}, s_{trans}, s_{occ}, s_{dim}, s_{col}) = \\ (\lambda_R s_{rot} + \lambda_T s_{trans} + \lambda_O s_{occ}) \times s_{dim} \times s_{col} \end{aligned} \quad (5)$$

for $\lambda_R, \lambda_T, \lambda_O > 0$.

After ordering the grasps according to their grasp prioritization score, the actual grasp applied is the first one to be feasible when a plan is made from the current end-effector pose to the target grasp pose. This final step in the grasp identification process is shown in Figure 2(c). The visualizations for intermediate steps are shown in Figure 9.

6 Grasping Experiment Setup and Properties

To evaluate how well a PS-CNN based perception module translates to practice, four grasping experiments were designed and executed. The first experiment consists of the standard single-object grasping tests, with objects ranging from an in-class grasping set of 3D-printed primitive shapes to household object datasets replicating those from the literature (Chu et al. 2018; Morrison et al. 2018). The objects cover known and unknown types with diverse geometries and physical properties. It also tests the claim that synthetic training data generated from domain randomization over primitive shapes is rich enough for real-world use. Grasping outcomes across all the objects are aggregated for comparison to published methods that perform similar grasping tests. The second experiment studies the effect of varied camera angles ranging from 30 to 75 degrees, thereby testing robustness with respect to the camera viewpoint. The third is a clutter-based robustness test: a multi-object clearing task. The fourth experiment is a task-oriented grasping task where a specific primitive shape must be grasped, as would be done when performing a specific task with the object. It aims to illustrate that the proposed method could facilitate higher-level semantic grasping. This section describes the manipulator setup, the grasping test sets, and the experimental evaluation criteria.

6.1 Robotic Arm Experimental Setup and Parameters

The eye-to-hand robotic arm and RGB-D camera setup used for the experiments is shown in Figure 10. The camera to manipulator base frame is established based on an ArUco tag captured by the camera. Both the described PS-CNN pipeline and the implemented baseline methods are tested on this setup. For the training dataset, each grasp set contributed by a grasp family is discretized according to the dimensions of the gripper so that neighboring grasps are not too similar. For grasp ranking, the weights in (5) are set as: $\lambda_R = \lambda_T = 0.5$, $\lambda_O = 0.0025$. Open-loop execution is performed with the plan of the top grasp via MoveIt! (Görner et al. 2019). The total running time, including segmentation, shape fitting, grasp generation, collision checking, and path planning for a single object averages 2.69s, of which segmentation takes 0.31s.

6.2 Grasping Object Sets

Several object sets are used across the experiments. For comparison with recently published methods, the same or similar objects were obtained and used to define a named dataset class. The intent behind the experiments is to test the value of primitive shapes, and not the challenges associated to active depth sensor measurements, thus some objects with negative reflectance properties were covered (i.e., with paper

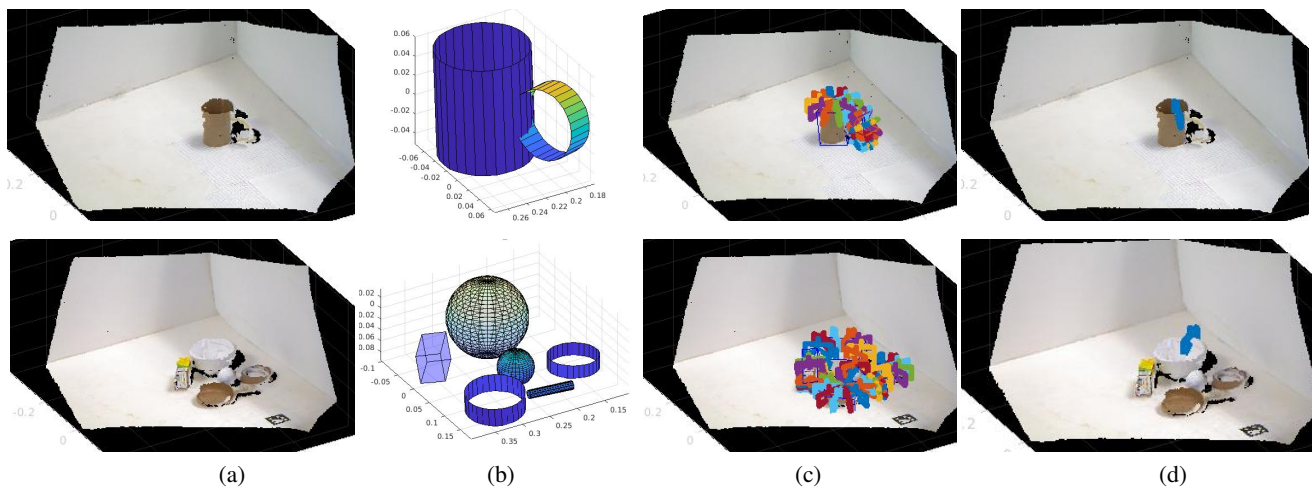


Figure 9. Sample visualization for candidate grasp generation, prioritization and selection on single object with multiple primitives (top) and multiple objects with multiple primitives (bottom). Shape decomposition, grasp candidates generation and grasp selection process are as follows. **(a)** Scene point cloud is reconstructed from depth input for visualization. **(b)** Target object is decomposed into a combination of primitive shapes given segmented depth input. **(c)** Grasp candidates are generated according to the estimated shape categories, poses and dimensions with invalid grasp eliminated. **(d)** The highest scored grasp is selected for final execution.



Figure 10. Experimental setup in the real-world.

or tape). The text below describes these object sets and identifies the corresponding visual in Figure 11.

Known Object Set. A set of 3D-printed shapes designed to match the training shapes parameter ranges is used for *known objects* testing and evaluation, Figure 11(a).

Varied Angle Grasping Set. The varied angle grasping set, seen in Fig. 11(b), comprises of 6 household objects which map to the 6 different primitive shapes classes.

Unknown Object Set. We collected objects to recreate the object sets used in Chu et al. (2018); Morrison et al. (2018), as shown in Figures 11(c,d). Chu’s set (Chu et al. 2018) includes ten commonly used objects collected from the Cornell Dataset, while Morrison’s set (Morrison et al. 2018) includes 12 household objects selected from the ACRV Picking Benchmark (APB) (Leitner et al. 2017) and the YCB Object Set (Calli et al. 2017).

Multi-object Grasping Set. To have a more diverse category of test objects, we combined all the unique objects in the

unknown object set, the primitive shapes set, and the task-oriented grasping set together. The object set has 31 objects in total, as shown in 11(e).

Task-oriented Grasping Set. To better illustrate the idea of shape decomposition, we collect 10 different household objects which could be decomposed into more than 1 primitive shape, see 11(f).

6.3 Grasping Evaluation Metrics

For the robotic arm testing, only the final outcomes of the grasping tests are scored. A run or attempt is considered to be a success if the target object is grasped, lifted, and held for at least 10 seconds. The scoring metric is the success rate (percentage). When possible, success rate percentages are accompanied by 95% confidence intervals where each grasp attempt is considered to be a binary variable following a binomial distribution.

7 Grasping Experiments and Results

This section covers the grasping experiments performed and discusses their outcomes in relation to existing work. The experiments test the hypothesis that decomposing objects into primitive shapes could contribute to a successful grasp recognition pipeline. They include primitive shape grasping, general object grasping, viewpoint robustness, and clutter robustness experiments. They highlight how effective shape is for establishing candidate grasps and how shape may complement existing methods. Lastly, there is a task-oriented grasping experiment based on the premise that different shape components perform different functions and should be grasped in accordance to intended use. Task-oriented grasping creates a pathway for a long-term investigation into shape as a mechanism to support task-specialized grasping beyond pick-and-place testing. Each experiment includes experimental setup details and testing criteria for context.



Figure 11. Object sets used for grasp experiments: (a) the known object set (3D-printed primitive shapes); (b) the varied angle set; (c) the unknown object set (Chu et al. 2018); (d) the unknown object set (Morrison et al. 2018); (e) the multi-object grasping set; (f) the task-oriented grasping set.

7.1 Static Object Grasping

The static object grasping experiment evaluates the proposed primitive shapes grasping recognition pipeline under an ideal setup. This section explores the following questions: 1) Does PS-CNN bridge the simulation-reality gap? 2) Is the primitive shapes concept robust to objects of different type or form? 3) What value does the primitive shapes idea have relative to other approaches to grasping?

The use of depth instead of RGB image inputs should minimize the sim2real gap when dense depth imagery is available as an input source and mostly captures the objects of interest. This expectation has been observed to hold for other depth-only methods, such as Viereck et al. (2017). Testing starts with the easiest case of *known objects*, i.e., 3D-printed primitive shapes. It continues with grasping experiments for the Chu and Morrison datasets (Chu et al. 2018; Morrison et al. 2018), containing *unknown objects*. The two sets cover representative household objects of different sizes and shapes. Lastly, aggregate results permit rough comparison with published works.

7.1.1 Known Objects (Primitive Shapes). The outcomes for the *known objects* grasping test are in Table 3. The baseline implementations include Jain and Argall (2016), a primitive-shape-based grasping system for household objects fitting spherical, cylindrical, and box-like shape primitives; and Chu et al. (2018), a typical 2D grasp representation approach. Also included is the previous primitive shape effort PS-CNN v1 (Lin et al. 2020).

The Jain and Argall (2016) baseline performed better for shapes easily approximated by spherical, cylindrical, and box-like primitives (83.3%), but performed worse otherwise (60.0%). When considering the 95% confidence interval of PS-CNN v2, all of the baseline methods were below the

interval’s lower bound. The improvements to PS-CNN v2 led to a 6.6% performance boost over PS-CNN v1. The primary factor behind the performance difference is the upgraded post-segmentation shape-fitting approach.

7.1.2 Unknown Objects. The outcomes for the *unknown objects* grasp test are in Tables 4 and 5. Included are published results of the analogous trials for the corresponding baseline methods (Chu et al. 2018; Morrison et al. 2018; Xu et al. 2021). For compatibility with the PS-CNN processing pipeline, the Chu et al. (2018) results are from the top-1 grasp selection criteria.

The first observation is that PS-CNN v2 has a 5.3% and a 3.3% drop in success rate relative to the *known objects* performance outcomes, for the Chu and Morrison datasets, respectively. Combining the 19 unique results from Tables 4 and 5, PS-CNN v2 has a 93.2% success rate, which is a 5.1% drop in performance. The drop does indicate some sensitivity to unknown objects, however the relative performance of PS-CNN v2 to the baseline methods indicates that the sensitivity is not large. PS-CNN v2 lies within the 95% confidence interval of the best performing method, GKNet, across the two datasets. Furthermore, it outperforms the source implementations from each of the datasets. The PS-CNN v2 confidence interval for the Chu dataset excludes Chu et al. (2018), which means that it is a more effective method. For the Morrison dataset, the confidence interval includes the source implementation but PS-CNN v2 has higher performance (by 1.3%).

GKNet (Xu et al. 2021) achieves the best performance on the two datasets individually, and when considering the 19 unique outcomes (95.3%). First, the performance difference is 3.2% (95.3% vs. 92.1%), which is lower than the baseline methods outside of GKNet, indicating that shape information can be effective at informing grasp options.

Table 3. Physical Grasping with 95% confidence intervals on Primitive Shapes (Known)

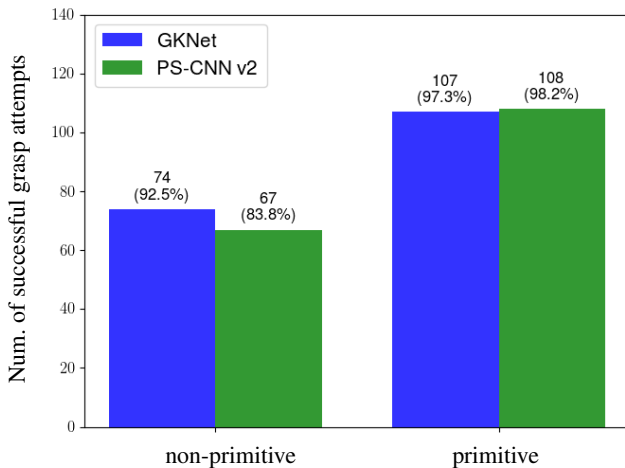
	Jain and Argall (2016)	Chu et al. (2018)	PS-CNN v1	PS-CNN v2
Cuboid	8/10	5/10	8/10	10/10
Cylinder	9/10	8/10	10/10	10/10
Semi-sphere	5/10	7/10	9/10	10/10
Stick	7/10	6/10	10/10	10/10
Ring	6/10	5/10	9/10	9/10
Sphere	8/10	8/10	9/10	10/10
Average (%)	71.7 ± 11.4	65.0 ± 12.1	91.7 ± 7.0	98.3 ± 3.3

Table 4. Physical Grasping for Chu’s Household Set, with 95% confidence intervals

object	Chu et al. (2018)	GKNet	PS-CNN v2
Banana	7/10	10/10	10/10
Glasses	8/10	10/10	8/10
Ball	9/10	10/10	10/10
Tape	10/10	9/10	10/10
Screwdriver	7/10	10/10	10/10
Stapler	10/10	9/10	9/10
Spoon	9/10	10/10	10/10
Bowl	10/10	10/10	10/10
Scissors	8/10	9/10	8/10
Mouse	8/10	9/10	8/10
Average (%)	86.0 ± 6.8	96.0 ± 3.8	93.0 ± 5.0

Table 5. Physical Grasping for Morrison’s Household Set, with 95% confidence intervals

object	Acc.	object	Acc.
Mug	10/10	Ball	10/10
Brush	10/10	Toothbrush	9/10
Bear toy	8/10	Dice	10/10
Tape	10/10	Duck toy	9/10
Marker	9/10	Clamp	7/10
Screwdriver	10/10	Cable	10/10
PS-CNN v2	93.3 ± 4.5 (%)		
Morrison et al. (2018)	92.0 ± 4.9 (%)		
GKNet	95.0 ± 3.9 (%)		

**Figure 12.** Comparison between GKNet (Xu et al. 2021) and PS-CNN v2 on the unknown object sets, where the 19 unique objects are divided into non-primitive shape-like ones and primitive shape like ones (The number in the bracket represents the corresponding success rate).

GKNet was trained with a variety of objects, some of which look like the test objects, thus it is expected to have some advantage. These objects are unknown to the PS-CNN but some are known to the GKNet. Secondly, the results are better interpreted by dividing the objects into two groups: non-primitive shape and primitive shape objects. Primitive shape objects are those that mostly fit one of the primitive shapes known to PS-CNN. As shown in Figure 12, GKNet outperforms PS-CNN v2 on the first group while PS-CNN v2 outperforms GKNet on the second group (e.g., they lack complex geometry). There exists the opportunity to combine both primitive shape and keypoint strategies to improve

general purpose grasping. Evidence for this can be seen through a composite GKNet+PS-CNN v2 success rate as obtained from selecting the maximum success rate between GKNet and PS-CNN v2. The composite success rate is 96.84%, which is 1.58% higher than GKNet and 4.74% higher than PS-CNN v2. Shape can play a complementary role to existing methods.

To understand some of the lower performing outcomes, this paragraph reviews a couple of prominent failure cases. The scissors in the Chu dataset should be grasped well since the cutting parts take the geometry of a stick when closed. Unfortunately, in some cases the flatness of the object exposed depth resolution issues. Figure 13 shows the color and depth images for a pair of scissors. The depth variation in the image is not as salient as the color variation, for the scissors relative to the background. Objects in the monocular depth image may be missing, have missing parts, or ambiguous geometry after denoising. Another example includes the clamp from the Morrison dataset, depicted in Figure 14. It has an irregular shape, which is challenging to be abstracted or decomposed, though the handles are stick-like. The algorithm does abstract part of the clamp as a stick, but does so for the wrong region. In spite of that, the grasp prediction seems visually reasonable, but the manipulator failed to grasp the object. This is attributed to the gripper geometry, which is wider than the typical parallel-plate gripper and more sensitive to imprecise gripper positioning. Compare the gripper used with the Franka Emika robot (Morrison et al. 2018), c.f. Figure 15. Other reduced grasping outcomes arise from shapes that don’t cleanly fit to the known primitive shape families, but do approximately fit to one primitive shape class. The best scoring grasp may not be best for the actual geometry, which opens the opportunity for

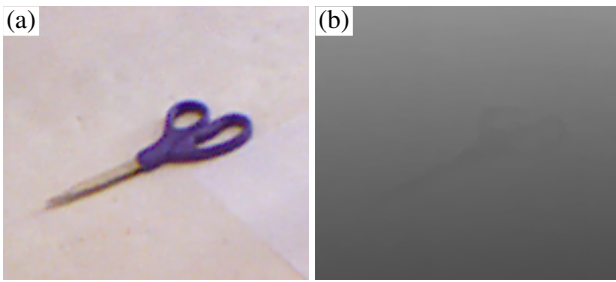


Figure 13. Scissor failure case. (a) Color image. (b) Depth input after post-processing. Object geometry has low signal-to-background differences.

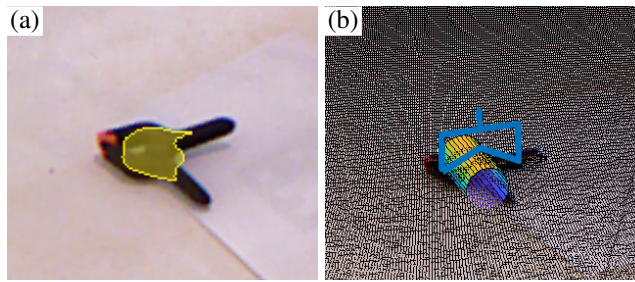


Figure 14. Clamp failure case. (a) Segmentation result. (b) Shape fitting result with rank-1 grasp. Though the grasp seems feasible, the wide end-effector affects grasping success.

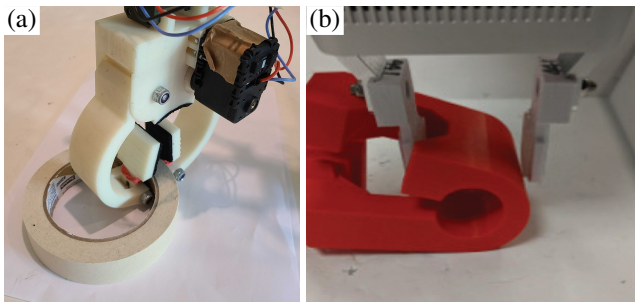


Figure 15. Comparison on the gripper between (a) ours and (b) the Franka Emika robot used in Morrison et al. (2018).

grasp quality scoring methods to provide improved scoring values over analytical models based on idealized geometries.

7.1.3 Tabletop Grasping of Individual Objects. To better place the value of primitive shapes relative to successful grasping strategies, the success rate statistics and experimental parameters were collected from published approaches employing only a single gripper (not suction-based).

Source Dataset and Setup: During the literature review, we noted the testing scenarios for the cited works and marked which publications provided physical robot grasping performance outcomes for individual objects on a tabletop. If single and multi-view results are provided, then the single view performance outcomes were taken. The references in Table 6 all performed such an experiment, except for Viereck et al. (2017) which used a single-camera visual servoing approach. Factors that cannot be accounted for include the robot manipulator and gripper, the software pipeline, and the actual test objects. Even though the test objects may differ, the general household object test sets tend to be similar. This is because recent research efforts obtain their sets from existing work (Calli et al. 2017) or attempt to recreate the object set (Chu et al. 2018; Morrison et al. 2018). The biggest exception being that Mahler et al. (2017); Morrison et al. (2018), and Xu et al. (2021) also take adversarial objects into consideration. In regard to the evaluation metric, most adopt a success policy similar to the one here, that is to successfully grasp and lift the object in the air. DexNet 2.0 (Mahler et al. 2017) has stricter criteria which only counts the grasps that are lifted, transported, and held the object after shaking the hand. Despite the existing differences, a rough comparison can still provide some context for the relative performance of PS-CNN v2 on household objects.

Presented in Table 6, the selected works are divided into two groups based on the grasp representation or strategy. One group (2D Grasp) typically employs a 2D grasp representation, processes the data in image-space, and assumes a top-down grasping technique. The second group (3D Grasp) employs a 3D grasp representation, processes the data using point clouds, and has less constraints on the grasp orientation or approach direction. PS-CNN belongs in the 3D Grasp group. Three key properties of the experiments are reported: the input type, the number of unique objects tested, and the total number of trials across the objects tested.

Outcome Analysis: Adopting the confidence interval of PS-CNN v2 as the selection criteria, we organize the top performing results sequentially: Viereck et al. (2017); Xu et al. (2021), PS-CNN v1, Wang et al. (2021), and Asif et al. (2017). They achieve a success rate higher than the lower bound of the PS-CNN v2 confidence interval (90.9%) while the remaining approaches lie below the interval and are presumed to achieve lower performance granted that their grasping experiments were comparable. PS-CNN v2 provides updated and improved success rates versus PS-CNN v1 based on an improved pipeline and evaluation on a larger test objects set.

Viereck et al. (2017) achieved the highest success rate among all. There are two possible reasons. The first being the limited quantity of test objects and trials, and the second being the advantage of the eye-in-hand visual servoing system design. The approach permits multiple estimates from different views over time, which may offset any grasp recognition errors associated to the grasp predictions of the initial image.

Xu et al. (2021) and Wang et al. (2021) focused on a compact grasp representation consisting of a left-right keypoint pair. Both achieved a good balance between accuracy and speed, which suggests an advantage of this smaller representation over the traditional 5-dimensional rectangle representation of 2D grasp methods. The earlier comparative analysis between GKNet and PS-CNN v2 suggests that combining the two methods should improve performance. In doing so, the keypoint representation may result in a faster processing pipeline since it would replace the current pose fitting process.

From Table 6, recent methods in the 2D Grasp group have a better success rate (over 90%) than methods in the 3D Grasp group (below 90%), with the exception of PS-CNN. The majority of the methods in the 3D Grasp group involve grasp sampling and anti-podal scoring methods.

Table 6. Grasping Comparison from Published Works

Approach	Settings			Success Rate (%)
	Inp.	Obj.	Trials	
2D Grasp				
Jiang et al. (2011)	M	12	-	87.9
Lenz et al. (2015)	M	30	100	84.0/89.0*
Pinto and Gupta (2016)	RGB	15	150	66.0
Johns et al. (2016)	D	20	100	80.3
Watson et al. (2017)	M	10	-	62.0
Mahler et al. (2017)	D	10	50	80.0
Asif et al. (2017)	M	35	134	91.9
Viereck et al. (2017)	D	10	40	97.5
Morrison et al. (2018)	D	20	200	87.0
Chu et al. (2018)	M	10	100	89.0
Satish et al. (2019)	D	8	80	87.5
Asif et al. (2019)	M	-	>200	89.0/90.0**
Lu et al. (2020)	M	10	30	84.0
Wang et al. (2021)	RGB	43	129	93.0
Xu et al. (2021)	M	30	300	95.3±2.4
3D Grasp				
Kopicki et al. (2016)	PC	45	45	77.8
ten Pas and Platt (2018)	PC	30	214	85.0
Liang et al. (2019)	PC	10	100	82.0
Mousavian et al. (2019)	PC	17	51	88.0
Lou et al. (2020)	PC	5	50	82.5
Wu et al. (2020)	PC	20	60	85.0
PS-CNN v1	D+PC	10	100	94.0
Lundell et al. (2021)	M	10	-	60.0
PS-CNN v2	D+PC	33 [†]	330	94.2±3.3

M: RGB-D; D: Depth; PC: Point cloud.

* Success rate of 84% / 89% achieved on Baxter / PR2 robot.

** Success rate of 89% / 90% achieved on ResNet and DenseNet.

[†] Combines the unique objects from Tables 3, 4, 5, and 9.

The reduced performance relative to PS-CNN suggests that the grasp sampling strategy may not be densely sampling the feasible grasp pose space. Evidence for this is comes from the top performing 2D method Viereck et al. (2017), which employs randomized grasp sampling. Moving from 2D to 3D grasp sampling induces a performance gap for the 3D Grasp methods. PS-CNN uses pre-determined grasp families from which grasps are densely sampled in the grasp family’s parameter space. It also operates with a performance comparable to top single-view 2D Grasp methods. Interestingly, these 2D Grasp methods are based on hypothesizing candidate anti-podal pairs Xu et al. (2021); Wang et al. (2021) as opposed to scoring randomly sampled grasp poses, or on scoring grasps when given the equivalent of an anti-podal pair. Incorporating these techniques into the PS-CNN network as a separate grasp prediction and evaluation branch may support enhanced grasping.

Overall, PS-CNN v2 achieves a success rate of 94.2% and is amongst the top performing methods. Testing over a variety of objects validates the generality and consistency of the PS-CNN pipeline. The success rate confirms the hypothesis that explicit shape recovery can inform how objects should be grasped. PS-CNN uses deep learning to segment the scene, after which the remaining pipeline follows traditional point-cloud, model-based fitting

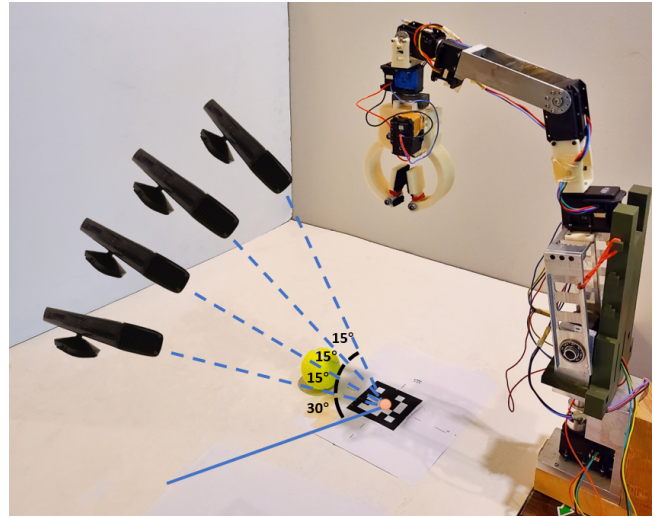


Figure 16. Experimental setup for grasping at varied camera angles (side view), where objects are tested under 30°, 45°, 60° and 75°, respectively.

and processing approaches. Consequently, there is an opportunity to include additional deep learning components for predicting grasp poses conditioned on the segmentation masks, and to include grasp quality scoring.

7.2 Grasping at Varied Camera Angles

The PS-CNN v2 deployment assumes a particular viewpoint similar to that of a human looking down towards a manipulation workspace. The training model included randomization for robustness to viewpoint variance, since it is not always the case that the a given deployment scenario can exactly match the training scenario. This section evaluates grasping consistency of PS-CNN v2 under varied camera angles.

7.2.1 Setup. This experiment focuses on grasping a single isolated object under different camera viewing angles. As is shown in Figure 16, the view angles vary from 30° to 75° in 15° increments, while the distance from the object to the camera frame is kept constant across the experiments. The view angle does not go below 30° since the effective working area of the Kinect would be too small under such settings. We do not test objects above 75° because the viewpoint fails to capture sufficient information regarding the sides of objects, which means that shape is difficult to infer and the limited point cloud information leads to degraded model fitting. The six objects tested match to different primitive shape classes.

7.2.2 Outcome Analysis and Discussion. As seen in Table 7, PS-CNN v2 grasping success rates for 30° and 60° lie within the 95% confidence interval of the 45° case, which demonstrates that PS-CNN v2 has robustness to the camera view within $45° \pm 15°$. Recall that the principle angle of the camera is set to be 42.3° in the simulation environment (Section 4.1). The 75° case lies outside of the 95% confidence interval, indicating a non-negligible reduction in performance. Nevertheless, performance continues to be competitive relative to methods found in Table 6. The performance drop is mainly due to the wrench, which is a flat and thin object lying on the ground. This case is illustrated

Table 7. Grasping at varied camera angles with 95% confidence intervals on our household set

object	Accuracy (%)			
	30°	45°	60°	75°
Bowl	10/10	9/10	10/10	10/10
Tape	10/10	10/10	10/10	10/10
Juice box	10/10	10/10	9/10	9/10
Wrench	10/10	10/10	10/10	8/10
Cup	9/10	10/10	10/10	9/10
Tennis ball	9/10	10/10	10/10	10/10
Average (%)	96.7 ± 4.5	98.3 ± 3.3	98.3 ± 3.3	93.3 ± 6.3

for a pair of scissors in Figure 13, where the depth sensor cannot retrieve a good depth map due to depth resolution limits. Depth-based approaches may benefit from precise estimation and isolation of the tabletop plane from the target object so that short or flat objects on the surface can be distinguished.

7.3 Multi-Object Grasping

To gauge how effective the PS-CNN pipeline is at grasping in clutter, a picking task was implemented with two modes denoted: light clutter and heavy clutter. Based on the training data and grasp scoring mechanism, light clutter should not significantly impact success rate, however heavy clutter might. The picking task setup was modeled after existing published works to allow for comparative evaluation.

7.3.1 Setup. From the set of 31 unique objects of the Multi-object Grasping Set depicted in Figure 11(e), a smaller set of 5 (or 10) objects are randomly selected and placed on the workspace close to each other with random poses, see Figure 17. For each grasp attempt trial, PS-CNN will first capture a depth image of the scene as the input and then predict the top-1 grasp candidate for each shape. Afterwards, the robot will only execute the grasp command with the highest grasp score across the scene. Following Ni et al. (2019), the robot has $n + 2$ grasp attempts to remove the objects. The experiment terminates when all objects have been picked or the robot has tried 7 (or 12) times.

7.3.2 Evaluation. The Multi-Object Grasping experiment involves three evaluation metrics, including: (1) **Success Rate (S)**: the percentage of grasp attempts that successfully grasp the target; (2) **Object Clearance Percentage (OC)**: the ratio of number of objects has been grasped successfully to the total number of objects in the scene; (3) **Completion percentage (C)**: marked as 1 if all the objects in the scene have been grasped successfully or 0 if any object was not picked. Table 8 compares these statistics to other published works. There are some differences regarding trial termination criteria (TC), with kG signifying up to k grasp attempts, $+k$ signifying $n + k$ allowed grasps for n objects, and $kSeq$ meaning k sequential failures. Ordering of the results is from least strict to strictest termination criteria, in terms of permitting the most amount of incorrect grasps before termination.

7.3.3 Light Clutter Grasping (5 Objects). As recorded in Table 8, the performance outcomes of PS-CNN v2 improved

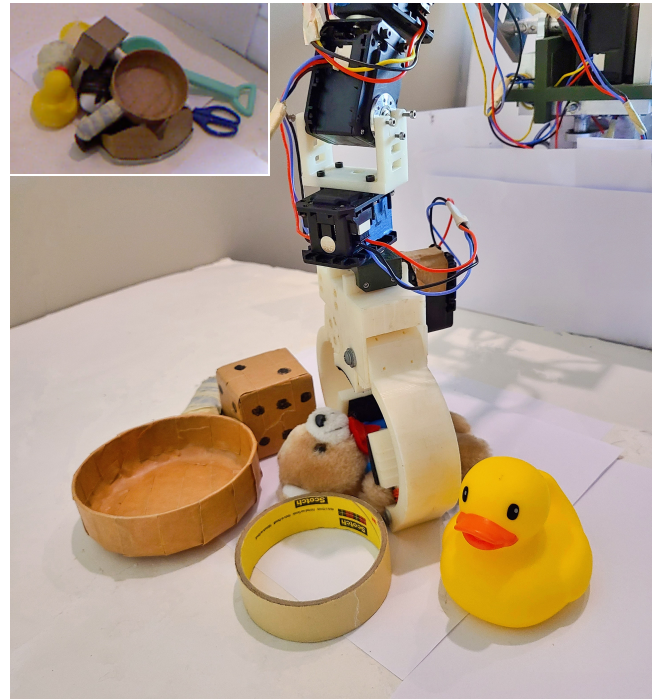


Figure 17. Setup of the multi-object grasping experiment. Objects are placed close to each other in the depicted 5 object, light clutter case. The top-left inset image shows the 10 object, heavy clutter case where objects are piled.

relative to v1. Importantly the object clearance and the completion percentage increased to 100%, indicating success for all of the object picking and clearing trials. Referring to the isolated object grasping results in Table 6 as a normative grasp success rate, the drop in grasp success rate under clutter for PS-CNN v2 is 1.4%, which indicates that the method is robust to light clutter. The grasp success rate lies within the 95% confidence interval of the single object case. Looking at the other rows, PS-CNN v2 performs as well as the top performing grasping methods noted. It matches the performance of Mahler et al. (2017) and Mahler and Goldberg (2017), also known as DexNet 1.0 and DexNet 2.0. These two methods were explicitly designed to handle grasping in cluttered scenarios and are sampled-based, deep network grasp quality scoring methods with a top-down grasping assumption. In contrast, PS-CNN v2 employs more traditional grasp scoring, which indicates that the primitive shape segmentation does a good job at isolating distinct regions likely to have good candidate grasp options. PS-CNN v2 performs similar to, but slightly higher than, GKNet (Xu et al. 2021). GKNet is a 2D grasp prediction strategy trained on manually annotated data of single objects. It employed a grasp scoring method similar to that of PS-CNN v2. These two methods perform comparably when tasked to grasp in clutter. As noted in Section 7.1, a composite GKNet+PS grasping strategy may provide complementary strengths and boost performance.

7.3.4 Heavy Clutter Grasping (10 Objects). As a stress test, picking tests with 10 objects piled together were also performed, see Figure 17 inset. The footprint of the pile was approximately equal to the footprint of the five Light Clutter objects. The DexNet variants (Mahler et al. 2017; Mahler and Goldberg 2017) should continue to be an upper

Table 8. Multi-Object Grasping Comparison

Method	#Obj.	#Sel.	#Trials	TC*	S#	OC [†]	C [‡]
Pinto and Gupta (2016)	21	10	5	None	38.0	100.0	100.0
Mahler et al. (2017)	25	5	20	5Seq	92.0	100.0	100.0
	25	10	10	5Seq	83.0	98.0	-
Mahler and Goldberg (2017)	25	5	20	5Seq	94.0	100.0	100.0
	25	10	10	5Seq	89.0	100.0	100.0
Xu et al. (2021)	30	5	20	5Seq	92.1	100.0	100.0
	30	10	10	5Seq	72.1	98.0	80.0
Gualtieri et al. (2016)	10	10	15	3Seq	84.0	77.0	-
Levine et al. (2018)	25	25	4	31G	82.1	99.0	75.0
Ni et al. (2019)	16	8	15	+2	86.1	87.5	-
PS-CNN v1 (2020)	10	5	10	+2	88.9	96.0	80.0
Corsaro et al. (2021)	29	13	10	+2	80.8	80.8	-
PS-CNN v2	31	5	20	+2	93.5	100.0	100.0
	31	10	5	+2	82.8	96.0	60.0

* TC = Termination Criteria.

S = Success Rate (%).

† OC = Object Clearance Percentage (%).

‡ C = Completion percentage (%).

bound reference on performance since their deep networks are trained to handle cluttered scenes. The performance drop for PS-CNN v2 is more acute here and lies outside of the 95% confidence interval for single object grasping. The grasping pipeline starts to break down. One reason is that the point clouds for the primitive shape regions are sparser under heavy clutter versus light clutter, due to occlusion. The shape fitting algorithm starts to exhibit sensitivity to the point cloud data and the model estimates lose accuracy. In comparison to other methods with the $n + 2$ termination criteria (Ni et al. 2019; Corsaro et al. 2021), PS-CNN v2 performs well. It has a higher object clearance rate compared to these two strategies while having a grasping success rate in between the two methods. Both are grasp sampling and scoring methods. PS-CNN v2 performs close to DexNet 1.0 (Mahler et al. 2017) which provides evidence that shape can serve as a strong prior for where to look for grasp candidates, even in clutter. However, it has a clear performance gap relative to DexNet 2.0 (Mahler and Goldberg 2017) indicating that there is a limit to shape alone when occlusion and clutter begin to reduce the information content and region continuity of primitive shape data in the depth image. Incorporating scoring methods robust to clutter, as a separate branch or subsequent process, should improve performance. We could not test the combination of PS-CNN with a downstream grasp quality CNN (GQ-CNN), such as DexNet. The publicly available version of Dex-Net does not provide the API to do so.

Lastly, one other source of picking failure was the actual gripper geometry versus the grasp scoring collision geometry. Rather than being a parallel-plate gripper, it has a jaw-like design, as captured in Figure 15(a). The swept volume of the gripper when closing is not perfectly modeled by the grasp ranking algorithm, resulting in false positives and false negatives. The former lead to the gripper colliding with other objects during execution, while the latter reject good candidates in favor of poorer candidates. The value of DexNet-like learning methods is the existence of training data based on the actual gripper geometry that better captures its effect on grasping performance.

7.4 Task-Oriented Grasping

The added value of segmenting objects according to shape is that the distinct shape regions may correspond to grasp preferences based on the task sought to accomplish. All of the previous experiments discussed focus on task-free grasping (or simply pick-n-place operations). This is because the methods do not differentiate object regions. Awareness of shape moves grasp selection one step closer to semantically meaningful and task appropriate grasping.

In this set of tests, each connected primitive shape region for the given object is presumed to correspond to a specific functional part. Grasping tests will compare task-free grasping to task-oriented grasping. In task-oriented grasping a specific region must be grasped based on the functionality of the object being grasped. Figure 18 depicts the depth and color images of a mug. Task-free grasping would focus any graspable part of a target object, which would include the container part and the handle. Task-oriented grasping would prefer to grasp the handle, Figure 18(d), behaving like humans would under certain use cases.

7.4.1 Setup. The methodology is similar to the static object grasping experiment (Section 7.1). The test set objects, depicted in Figure 11(f), each consist of more than one functional part or primitive shape category, one of which is defined to be the task-oriented preference when grasping.

7.4.2 Outcome Analysis and Discussion. Only Jain and Argall (2016) and PS-CNN v1 were tested as baselines since they are shape-based. Table 9 reports the performance of the systems on the grasping tests. The method in Jain and Argall (2016) simply approximates each object with a single primitive shape. which renders task-oriented grasping inapplicable. The inability to capture all of the primitive shape sub-components in the objects tested degraded this method’s performance relative to the case when objects were uniquely a single primitive shape class, see Table 3 (a 6.7% drop in success rate). In contrast PS-CNN v1 and v2 performed closer to their nominal performance for single primitive shape class objects. This demonstrates the ability of the PS-CNN pipeline to capture the primitive shapes and

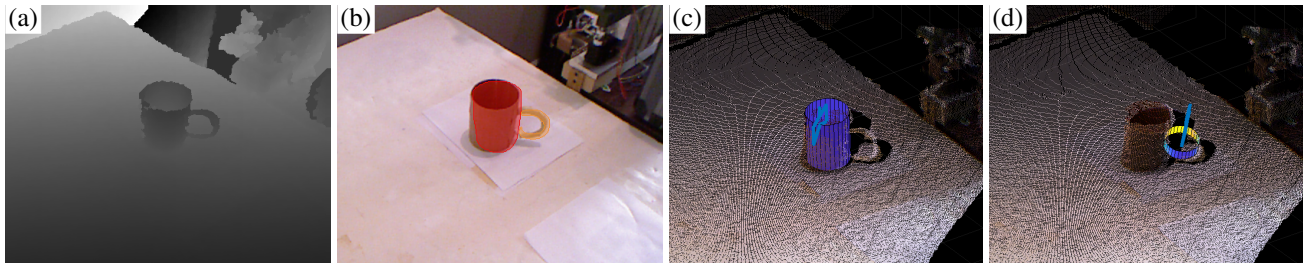


Figure 18. Task-oriented grasping. (a) Depth input. (b) Segmented mask. (c) Primitive shape model and grasp candidate on main body. (d) Primitive shape model and grasp candidate on handle.

Table 9. Task-Free and Task-Oriented Grasping with 95% confidence intervals

Target Objects	Task-Free			Task-Oriented	
	Jain and Argall (2016)	PS-CNN v1	PS-CNN v2	PS-CNN v1	PS-CNN v2
Mug	6/10	9/10	10/10	9/10	10/10
Pot	3/10	10/10	10/10	8/10	10/10
Pan	5/10	10/10	10/10	8/10	9/10
Brush	5/10	6/10	10/10	4/10	9/10
Handbag	9/10	10/10	10/10	8/10	10/10
Hammer	9/10	9/10	10/10	7/10	9/10
Basket	6/10	10/10	10/10	8/10	9/10
Bucket	7/10	8/10	9/10	8/10	8/10
Shovel	8/10	10/10	10/10	9/10	10/10
Net spoon	7/10	10/10	9/10	8/10	8/10
Average (%)	65.0 ± 9.3	92.0 ± 5.3	97.0 ± 3.3	73.0 ± 8.7	93.0 ± 4.9

select the best one to use for grasping based on the specified scoring mechanism.

When moving to the task-oriented case PS-CNN v2 has a clear advantage over PS-CNN v1. Not only is the task-free success rate higher, but the performance drop in the task-oriented case is lower, at a 4% drop versus a 19% drop. The improved training corpus and upgraded shape fitting module contributed to the performance boost. The difference is best observed for the brush test object, which had the largest improvement for the task-free and task-oriented cases. Figure 19(a,c) shows that PS-CNN v1 failed to distinguish the handle and the base of the brush while PS-CNN v2 could differentiate the two regions. The improvements suggest that more research placed on the precision grasping of specific object parts or regions can contribute to improved general purpose grasping. Additionally, the ability to achieve task-oriented grasping through shape differentiation permits follow-up investigations into realizing more advanced semantic grasping.

8 Conclusion

This paper investigated the value of primitive shape awareness for robotic grasping. To that end, it described a segmentation-based shape primitive grasping pipeline that leverages recent advances in deep learning to decompose objects into multiple primitive shapes regions then recover their corresponding shape models. Prior knowledge of the shape primitive permits dense generation of grasp configurations from shape-specific, parametrized grasp families. Once the primitive shape object regions are known, the pipeline employs classical grasping paradigms to filter, rank, and execute the grasp operation. The primitive shapes

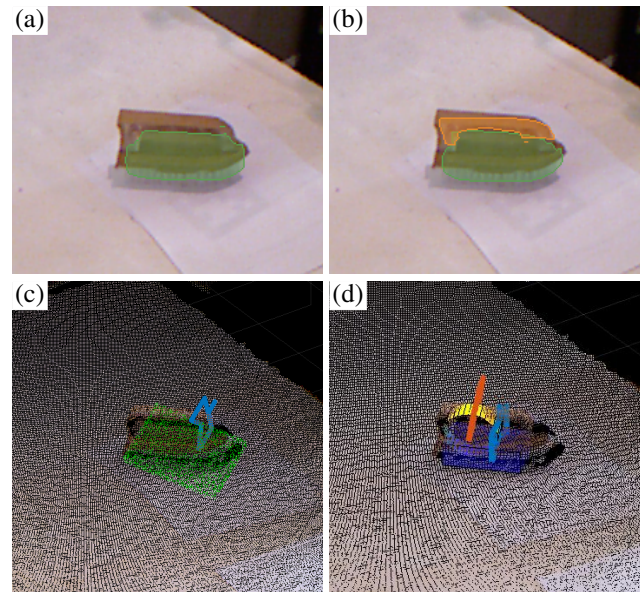


Figure 19. Comparison between PS-CNN v1 and v2 on the brush. (a) Segmentation from v1. (b) Segmentation from v2. (c) Top grasp candidate of v1. (d) Top grasp candidates of v2.

deep network (PS-CNN) shows that high-performance grasp candidates can be learned from simulated visual data of primitive shapes without collecting a large-scale dataset of CAD models and simulating grasp attempts.

In static object grasping experiments, PS-CNN-enabled grasping achieves a 94.2% grasp success rate amongst the top-performing methods. Multi-object grasping in light clutter (5 objects per scene) has a 93.5% grasp success rate and a 100% completion rate. Grasping trials with the camera

set at varied angles quantifies robustness to view angles. These outcomes indicate that PS-CNN successfully bridges the gap between the synthetic primitive shape training data and real-world test objects, showing generalizability to different object types or forms. Moreover, our segmentation-based approach facilitates task-specific grasping on the objects composed of multiple shapes that have functional meaning or purpose. It goes beyond simple pick-and-place testing since there is semantic meaning behind grasp constraints. Grasping experiments show a 97% grasp success rate in task-free grasping and 93% for task-oriented grasping. More advanced tasks could be enabled through task-aware grasping strategies, including human-robot interaction tasks.

PS-CNN is a first attempt to use deep networks to explicitly extract an object's primitive shape composition for grasping. Consequently, there is room to improve. The first direction is regarding the performance gap between objects matching to known primitive shapes versus objects with non-primitive or more complex geometry. The second is regarding the trade-off between precision and speed, as PS-CNN takes 2.69s to generate a grasp plan per object on average. The bottleneck lies in the RANSAC-based shape fitting part, where tens of thousands of proposals are filtered and ranked. A better idea would be to leverage the power of deep networks to predict rough pose and sizes as the initialization. In doing so, these modifications have the potential to further improve the grasping success rate by including related grasping tasks, such as grasp prediction and scoring, as additional task-related deep network branches.

To promote exploration into primitive shapes and reproduction of outcomes, the source code is publicly available (Lin et al. 2021).

Funding

This work supported in part by the National Science Foundation under Award #1605228 and #2026611. Any opinions, findings, and conclusions or recommendations expressed in this material are those of the author(s) and do not necessarily reflect the views of the National Science Foundation.

References

- Aleotti J and Caselli S (2012) A 3D shape segmentation approach for robot grasping by parts. *Robotics and Autonomous Systems* 60(3): 358–366.
- Andrychowicz OM, Baker B, Chociej M, Jozefowicz R, McGrew B, Pachocki J, Petron A, Plappert M, Powell G, Ray A et al. (2020) Learning dexterous in-hand manipulation. *International Journal of Robotics Research* 39(1): 3–20.
- Asif U, Bennamoun M and Sohel FA (2017) RGB-D object recognition and grasp detection using hierarchical cascaded forests. *IEEE Transactions on Robotics* 33(3): 547–564.
- Asif U, Tang J and Harrer S (2019) Densely supervised grasp detector (DSGD). In: *AAAI Conference on Artificial Intelligence*, volume 33. pp. 8085–8093.
- Attene M and Patanè G (2010) Hierarchical structure recovery of point-sampled surfaces. In: *Computer Graphics Forum*, volume 29. pp. 1905–1920.
- Bicchi A and Kumar V (2000) Robotic grasping and contact: A review. In: *IEEE International Conference on Robotics and Automation*, volume 1. pp. 348–353.
- Bohg J, Morales A, Asfour T and Kragic D (2014) Data-driven grasp synthesis—A survey. *IEEE Transactions on Robotics* 30(2): 289–309.
- Caldera S, Rassau A and Chai D (2018) Review of deep learning methods in robotic grasp detection. *Multimodal Technologies and Interaction* 2(3): 57.
- Calli B, Singh A, Bruce J, Walsman A, Konolige K, Srinivasa S, Abbeel P and Dollar AM (2017) Yale-CMU-Berkeley dataset for robotic manipulation research. *International Journal of Robotics Research* 36(3): 261–268.
- Chen DY, Tian XP, Shen YT and Ouhyoung M (2003) On visual similarity based 3d model retrieval. In: *Computer graphics forum*, volume 22. pp. 223–232.
- Chu F, Xu R and Vela PA (2018) Real-world multiobject, multigrasp detection. *IEEE Robotics and Automation Letters* 3(4): 3355–3362.
- Community BO (2018) *Blender - A 3D modelling and rendering package*. Blender Foundation, Stichting Blender Foundation, Amsterdam.
- Corsaro M, Tellex S and Konidaris G (2021) Learning to detect multi-modal grasps for dexterous grasping in dense clutter. *IEEE/RSJ International Conference on Intelligent Robots and Systems* : 4624–4630.
- Danielczuk M, Matl M, Gupta S, Li A, Lee A, Mahler J and Goldberg K (2019) Segmenting unknown 3D objects from real depth images using Mask R-CNN trained on synthetic data. In: *IEEE International Conference on Robotics and Automation*. pp. 7283–7290.
- Denninger M, Sundermeyer M, Winkelbauer D, Zidan Y, Olefir D, Elbadrawy M, Lodhi A and Katam H (2019) Blenderproc. *arXiv preprint arXiv:1911.01911* .
- Depierre A, Dellandréa E and Chen L (2018) Jacquard: A large scale dataset for robotic grasp detection. In: *IEEE/RSJ International Conference on Intelligent Robots and Systems*. pp. 3511–3516.
- Eppner C and Brock O (2013) Grasping unknown objects by exploiting shape adaptability and environmental constraints. In: *IEEE/RSJ International Conference on Intelligent Robots and Systems*. pp. 4000–4006.
- Fang K, Zhu Y, Garg A, Kuryenkov A, Mehta V, Fei-Fei L and Savarese S (2018) Learning task-oriented grasping for tool manipulation from simulated self-supervision. In: *Robotics: Science and Systems*.
- Funkhouser T, Min P, Kazhdan M, Chen J, Halderman A, Dobkin D and Jacobs D (2003) A search engine for 3D models. *ACM Transactions on Graphics* 22(1): 83–105.
- Goldfeder C, Allen PK, Lackner C and Pelossof R (2007) Grasp planning via decomposition trees. *IEEE International Conference on Robotics and Automation* .
- Görner M, Haschke R, Ritter H and Zhang J (2019) MoveIt! task constructor for task-level motion planning. In: *IEEE International Conference on Robotics and Automation*. pp. 190–196.
- Gualtieri M, Ten Pas A, Saenko K and Platt R (2016) High precision grasp pose detection in dense clutter. In: *IEEE/RSJ International Conference on Intelligent Robots and Systems*. pp. 598–605.
- Hachiuma R and Saito H (2020) Pose estimation of primitive-shaped objects from a depth image using superquadric representation. *Applied Sciences* 10(16): 5442.

- He K, Gkioxari G, Dollár P and Girshick R (2017) Mask R-CNN. In: *IEEE International Conference on Computer Vision*. pp. 2961–2969.
- Hodaň T, Vineet V, Gal R, Shalev E, Hanzelka J, Connell T, Urbina P, Sinha SN and Guenter B (2019) Photorealistic image synthesis for object instance detection. In: *IEEE International Conference on Image Processing*. pp. 66–70.
- Holz D, Holzer S, Rusu RB and Behnke S (2011) Real-time plane segmentation using RGB-D cameras. In: *Robot Soccer World Cup*. pp. 306–317.
- Huebner K and Kragic D (2008) Selection of robot pre-grasps using box-based shape approximation. In: *IEEE/RSJ International Conference on Intelligent Robots and Systems*. pp. 1765–1770.
- Jain S and Argall B (2016) Grasp detection for assistive robotic manipulation. In: *IEEE International Conference on Robotics and Automation*. pp. 2015–2021.
- Jiang Y, Moseson S and Saxena A (2011) Efficient grasping from RGBD images: Learning using a new rectangle representation. In: *IEEE International Conference on Robotics and Automation*. pp. 3304–3311.
- Johns E, Leutenegger S and Davison AJ (2016) Deep learning a grasp function for grasping under gripper pose uncertainty. In: *IEEE/RSJ International Conference on Intelligent Robots and Systems*. pp. 4461–4468.
- Kaiser A, Ybanez Zepeda JA and Boubekeur T (2019) A survey of simple geometric primitives detection methods for captured 3D data. In: *Computer Graphics Forum*, volume 38. pp. 167–196.
- Kalogerakis E, Averkiou M, Maji S and Chaudhuri S (2017) 3D shape segmentation with projective convolutional networks. In: *IEEE Conference on Computer Vision and Pattern Recognition*. pp. 3779–3788.
- Kopicki M, Detry R, Adjigble M, Stolkin R, Leonardis A and Wyatt JL (2016) One-shot learning and generation of dexterous grasps for novel objects. *International Journal of Robotics Research* 35(8): 959–976.
- Leitner J, Tow AW, Sünderhauf N, Dean JE, Durham JW, Cooper M, Eich M, Lehnert C, Mangels R, McCool C et al. (2017) The ACRV picking benchmark: A robotic shelf picking benchmark to foster reproducible research. In: *IEEE International Conference on Robotics and Automation*. pp. 4705–4712.
- Lenz I, Lee H and Saxena A (2015) Deep learning for detecting robotic grasps. *International Journal of Robotics Research* 34(4-5): 705–724.
- Levine S, Pastor P, Krizhevsky A, Ibarz J and Quillen D (2018) Learning hand-eye coordination for robotic grasping with deep learning and large-scale data collection. *International Journal of Robotics Research* 37(4-5): 421–436.
- Li L, Sung M, Dubrovina A, Yi L and Guibas LJ (2019) Supervised fitting of geometric primitives to 3d point clouds. In: *IEEE Conference on Computer Vision and Pattern Recognition*. pp. 2652–2660.
- Liang H, Ma X, Li S, Görner M, Tang S, Fang B, Sun F and Zhang J (2019) PointNetGPD: Detecting grasp configurations from point sets. In: *IEEE International Conference on Robotics and Automation*. pp. 3629–3635.
- Lin Y, Tang C, Chu F and Vela P (2021) grasp_primitiveShapes. github.com/ivalab/grasp_primitiveShape.
- Lin Y, Tang C, Chu FJ and Vela PA (2020) Using synthetic data and deep networks to recognize primitive shapes for object grasping. In: *IEEE International Conference on Robotics and Automation*. pp. 10494–10501.
- Lou X, Yang Y and Choi C (2020) Learning to generate 6-DoF grasp poses with reachability awareness. In: *IEEE International Conference on Robotics and Automation*. pp. 1532–1538.
- Lu Q, Chenna K, Sundaralingam B and Hermans T (2020) Planning multi-fingered grasps as probabilistic inference in a learned deep network. In: *Robotics Research*. pp. 455–472.
- Lundell J, Corona E, Le TN, Verdoja F, Weinzaepfel P, Rogez G, Moreno-Noguer F and Kyrki V (2021) Multi-FinGan: Generative coarse-to-fine sampling of multi-finger grasps. In: *IEEE International Conference on Robotics and Automation*. pp. 4495–4501.
- Mahler J and Goldberg K (2017) Learning deep policies for robot bin picking by simulating robust grasping sequences. In: *Conference on Robot Learning*. pp. 515–524.
- Mahler J, Liang J, Niyaz S, Laskey M, Doan R, Liu X, Ojea JA and Goldberg K (2017) Dex-Net 2.0: Deep learning to plan robust grasps with synthetic point clouds and analytic grasp metrics. In: *Robotics: Science and Systems*.
- Mahler J, Matl M, Satish V, Danielczuk M, DeRose B, McKinley S and Goldberg K (2019) Learning ambidextrous robot grasping policies. *Science Robotics* 4(26): eaau4984.
- Margolin R, Zelnik-Manor L and Tal A (2014) How to evaluate foreground maps. In: *IEEE Conference on Computer Vision and Pattern Recognition*. pp. 248–255.
- Marr D and Nishihara HK (1978) Representation and recognition of the spatial organization of three-dimensional shapes. *Proceedings of the Royal Society of London. Series B. Biological Sciences* 200(1140): 269–294.
- Miller AT, Knoop S, Christensen HI and Allen PK (2003) Automatic grasp planning using shape primitives. In: *IEEE International Conference on Robotics and Automation*. pp. 1824–1829.
- Morrill N, Tremblay J, Lin Y, Tyree S, Birchfield S, Pascucci V and Wald I (2021) Nvisii: A scriptable tool for photorealistic image generation. *arXiv preprint arXiv:2105.13962*.
- Morrison D, Corke P and Leitner J (2018) Closing the Loop for Robotic Grasping: A Real-time, Generative Grasp Synthesis Approach. In: *Robotics: Science and Systems*.
- Mousavian A, Eppner C and Fox D (2019) 6-DoF GraspNet: Variational grasp generation for object manipulation. In: *IEEE International Conference on Robotics and Automation*. pp. 2901–2910.
- Mukherjee S et al. (2014) Study on performance improvement of oil paint image filter algorithm using parallel pattern library. In: *CS & IT Conference Proceedings*, volume 4.
- Murray RM (2017) *A mathematical introduction to robotic manipulation*.
- Ni P, Zhang W, Bai W, Lin M and Cao Q (2019) A new approach based on two-stream CNNs for novel objects grasping in clutter. *Journal of Intelligent & Robotic Systems* 94(1): 161–177.
- Ni P, Zhang W, Zhu X and Cao Q (2020) PointNet++ Grasping: Learning an end-to-end spatial grasp generation algorithm from sparse point clouds. In: *IEEE International Conference on Robotics and Automation*. pp. 3619–3625.
- Park D and Chun SY (2018) Classification based grasp detection using spatial transformer network. In: *arXiv preprint*

- arXiv:1803.01356*.
- Paschalidou D, Ulusoy AO and Geiger A (2019) Superquadrics revisited: Learning 3D shape parsing beyond cuboids. In: *IEEE Conference on Computer Vision and Pattern Recognition*. pp. 10344–10353.
- Paschalidou D, van Gool L and Geiger A (2020) Learning unsupervised hierarchical part decomposition of 3D objects from a single rgb image. *arXiv preprint arXiv:2004.01176*.
- Peng S, Liu Y, Huang Q, Zhou X and Bao H (2019) PVNet: Pixel-wise voting network for 6DoF pose estimation. In: *IEEE Conference on Computer Vision and Pattern Recognition*. pp. 4561–4570.
- Peng XB, Andrychowicz M, Zaremba W and Abbeel P (2018) Sim-to-real transfer of robotic control with dynamics randomization. In: *IEEE International Conference on Robotics and Automation*. pp. 1–8.
- Pinto L and Gupta A (2016) Supersizing self-supervision: Learning to grasp from 50k tries and 700 robot hours. In: *IEEE International Conference on Robotics and Automation*. pp. 3406–3413.
- Planche B, Wu Z, Ma K, Sun S, Kluckner S, Lehmann O, Chen T, Hutter A, Zakharov S, Kosch H et al. (2017) DepthSynth: Real-time realistic synthetic data generation from cad models for 2.5 D recognition. In: *International Conference on 3D Vision*. pp. 1–10.
- Prakash A, Boochoon S, Brophy M, Acuna D, Cameracci E, State G, Shapira O and Birchfield S (2019) Structured domain randomization: Bridging the reality gap by context-aware synthetic data. In: *IEEE International Conference on Robotics and Automation*. pp. 7249–7255.
- Prattichizzo D, Malvezzi M, Gabiccini M and Bicchi A (2012) On the manipulability ellipsoids of underactuated robotic hands with compliance. *Robotics and Autonomous Systems* 60(3): 337–346.
- Qin Y, Chen R, Zhu H, Song M, Xu J and Su H (2020) S4G: Amodal single-view single-shot SE (3) grasp detection in cluttered scenes. In: *Conference on Robot Learning*. pp. 53–65.
- Rohmer E, Singh SP and Freese M (2013) V-REP: A versatile and scalable robot simulation framework. In: *IEEE/RSJ International Conference on Intelligent Robots and Systems*. pp. 1321–1326.
- Rosales C, Suárez R, Gabiccini M and Bicchi A (2012) On the synthesis of feasible and prehensile robotic grasps. In: *IEEE International Conference on Robotics and Automation*. pp. 550–556.
- Sankaranarayanan S, Balaji Y, Jain A, Lim SN and Chellappa R (2018) Learning from synthetic data: Addressing domain shift for semantic segmentation. In: *IEEE Conference on Computer Vision and Pattern Recognition*. pp. 3752–3761.
- Satish V, Mahler J and Goldberg K (2019) On-policy dataset synthesis for learning robot grasping policies using fully convolutional deep networks. *IEEE Robotics and Automation Letters* 4(2): 1357–1364.
- Schnabel R, Wahl R and Klein R (2007) Efficient RANSAC for point-cloud shape detection. In: *Computer graphics forum*, volume 26. pp. 214–226.
- Sharma G, Liu D, Kalogerakis E, Maji S, Chaudhuri S and Měch R (2020) ParSeNet: A parametric surface fitting network for 3D point clouds. *arXiv preprint arXiv:2003.12181*.
- Shilane P, Min P, Kazhdan M and Funkhouser T (2004) The princeton shape benchmark. In: *Shape Modeling Applications*. pp. 167–178.
- Shiraki Y, Nagata K, Yamanobe N, Nakamura A, Harada K, Sato D and Nenchev DN (2014) Modeling of everyday objects for semantic grasp. In: *IEEE International Symposium on Robot and Human Interactive Communication*. pp. 750–755.
- Sparavigna AC and Marazzato R (2010) CLD-shaped brush-strokes in non-photorealistic rendering. In: *arXiv preprint arXiv:1002.4317*.
- Sweeney C, Izatt G and Tedrake R (2019) A supervised approach to predicting noise in depth images. In: *IEEE International Conference on Robotics and Automation*. pp. 796–802.
- ten Pas A, Gualtieri M, Saenko K and Platt R (2017) Grasp pose detection in point clouds. *International Journal of Robotics Research* 36(13-14): 1455–1473.
- ten Pas A and Platt R (2018) Using geometry to detect grasp poses in 3D point clouds. In: *Robotics Research*. Springer, pp. 307–324.
- Tobin J, Biewald L, Duan R, Andrychowicz M, Handa A, Kumar V, McGrew B, Ray A, Schneider J, Welinder P et al. (2018) Domain randomization and generative models for robotic grasping. In: *IEEE/RSJ International Conference on Intelligent Robots and Systems*. pp. 3482–3489.
- Tobin J, Fong R, Ray A, Schneider J, Zaremba W and Abbeel P (2017) Domain randomization for transferring deep neural networks from simulation to the real world. In: *IEEE/RSJ International Conference on Intelligent Robots and Systems*. pp. 23–30.
- Tremblay J, To T and Birchfield S (2018a) Falling things: A synthetic dataset for 3D object detection and pose estimation. In: *IEEE Conference on Computer Vision and Pattern Recognition Workshops*. pp. 2038–2041.
- Tremblay J, To T, Sundaralingam B, Xiang Y, Fox D and Birchfield S (2018b) Deep object pose estimation for semantic robotic grasping of household objects. In: *Conference on Robot Learning*. pp. 306–316.
- Tulsiani S, Su H, Guibas LJ, Efros AA and Malik J (2017) Learning shape abstractions by assembling volumetric primitives. In: *IEEE Conference on Computer Vision and Pattern Recognition*. pp. 2635–2643.
- Tung CP and Kak AC (1996) Fast construction of force-closure grasps. *IEEE Transactions on Robotics and Automation* 12(4): 615–626.
- Vezzani G, Pattacini U and Natale L (2017) A grasping approach based on superquadric models. In: *IEEE International Conference on Robotics and Automation*. pp. 1579–1586.
- Viereck U, Pas At, Saenko K and Platt R (2017) Learning a visuomotor controller for real world robotic grasping using simulated depth images. In: *Conference on Robot Learning*. pp. 291–300.
- Wang H, Sridhar S, Huang J, Valentin J, Song S and Guibas LJ (2019) Normalized object coordinate space for category-level 6D object pose and size estimation. In: *IEEE Conference on Computer Vision and Pattern Recognition*. pp. 2642–2651.
- Wang Y, Zheng Y, Gao B and Huang D (2021) Double-dot network for antipodal grasp detection. *IEEE/RSJ International Conference on Intelligent Robots and Systems*: 4631–4638.
- Watson J, Hughes J and Iida F (2017) Real-world, real-time robotic grasping with convolutional neural networks. In: *Real-world,*

- real-time robotic grasping with convolutional neural networks.* pp. 617–626.
- Wohlkinger W, Aldoma A, Rusu RB and Vincze M (2012) 3DNet: Large-scale object class recognition from cad models. In: *IEEE International Conference on Robotics and Automation.* pp. 5384–5391.
- Wu C, Chen J, Cao Q, Zhang J, Tai Y, Sun L and Jia K (2020) Grasp Proposal Networks: An end-to-end solution for visual learning of robotic grasps. *arXiv preprint arXiv:2009.12606* .
- Xia C, Zhang Y, Shang Y and Liu T (2018) Reasonable grasping based on hierarchical decomposition models of unknown objects. In: *International Conference on Control, Automation, Robotics and Vision.* pp. 1953–1958.
- Xiang Y, Schmidt T, Narayanan V and Fox D (2018) PoseCNN: A convolutional neural network for 6D object pose estimation in cluttered scenes. In: *Robotics: Science and Systems.*
- Xu R, Chu FJ and Vela PA (2021) GKNet: grasp keypoint network for grasp candidates detection. *arXiv preprint arXiv:2106.08497* .
- Yamanobe N and Nagata K (2010) Grasp planning for everyday objects based on primitive shape representation for parallel jaw grippers. In: *IEEE International Conference on Robotics and Biomimetics.* pp. 1565–1570.
- Zakharov S, Kehl W and Ilic S (2019) DeceptionNet: Network-driven domain randomization. *arXiv preprint arXiv:1904.02750* .
- Zeng A, Song S, Welker S, Lee J, Rodriguez A and Funkhouser T (2018) Learning synergies between pushing and grasping with self-supervised deep reinforcement learning. In: *IEEE/RSJ International Conference on Intelligent Robots and Systems.* pp. 4238–4245.